PENNSTATE

Applied Research Laboratory

Final Report to

NASA Langley Research Center

On

FREE-FIELD PROPAGATION OF HIGH INTENSITY NOISE

NASA Research Grant NAG-I-4

By

Joseph P. Welz and Oliver H. McDaniel
Principal Investigator: Dr. Oliver H. McDaniel

Period Covered

December 1, 1979 to February 28, 1983

The Noise Control Laboratory and
Applied Research Laboratory
The Pennsylvania State University

FORWARD

The experimental work documented in this report was performed at Penn State's Noise Control Laboratory in the College of Engineering. A significant portion of the report was written after Mr. Welz and Dr. McDaniel joined the Applied Research Laboratory. The body of the report is Mr. Welz' Master's Thesis in the Penn State Graduate Program in Acoustics.

ABSTRACT

Observed spectral data from supersonic jet aircraft are known to contain much more high frequency energy than can be explained by linear acoustic propagation theory. It is believed that the high frequency energy is an effect of nonlinear distortion due to the extremely high acoustic levels generated by the jet engines.

The objective of this research was to measure acoustic waveform distortion for spherically diverging high intensity noise. This objective was reached by using an electropneumatic acoustic source capable of generating sound pressure levels in the range of 140 to 160 decibels (re 20 μ Pa). The noise spectrum was shaped to represent the spectra generated by jet engines. Two microphones were used to capture the acoustic pressure waveform at different points along the propagation path in order to provide a direct measure of the waveform distortion as well as spectral distortion.

A secondary objective of this research was to determine that the observed distortion is an acoustic effect. To do this an existing computer prediction code that deals with nonlinear acoustic propagation was used on data representative of the measured data.

The results clearly demonstrate that high intensity jet noise does shift the energy in the spectrum to the higher frequencies along the propagation path. In addition, the data from the computer model are in good agreement with the measurements, thus demonstrating that the waveform distortion can be accounted for with nonlinear acoustic theory.

TABLE OF CONTENTS

LIST OF FIGURES

Figure | Page

LIST OF SYMBOLS

c_0	Adiabatic speed of sound
D_n	Normalized voltage level output by the spectrum analyzer
F_{max}	Spectrum analyzer's maximum frequency setting
$GAIN$	External amplification
G_{attn}	Spectrum analyzer's attenuator setting
k	Wave number, $= \frac{\omega}{c_0}$
p	Normalized acoustic pressure, $\left(\frac{r}{r_0}\right)\left(\frac{p'}{p_{max}}\right)$
P_n	Sound pressure of the n^{th} sample
p'	Peak pressure
r	Radial distance
r_0	Rayleigh distance
r_c	$r_0 e^{\left(\frac{1}{\sigma_0}\right)}$
T_n	Time of the n^{th} sound pressure measurement
V_m	Pressure measurement voltage
V_n	Voltage of the n^{th} sound pressure measurement
V_{cal}	Calibration voltage
W	Spectrum analyzer's time window
β	Nonlinearity factor, $\frac{C_p}{C_v}$ in air, $= 1.4$
ϵ	Peak Mach number
ω	Frequency
σ	Scaled range, $\beta * \epsilon * k * r_0 * \ln\left(\frac{r}{r_0}\right)$
τ	$\omega(t - \frac{r}{c_0})$

ACKNOWLEDGMENTS

The author would like to gratefully acknowledge his advisor, Dr. Oliver H. McDaniel, for his guidance, support, and especially his patience, throughout this research project. He is also grateful to Dr. Gerhard Reethof for the fine laboratory in which he was able to perform this research. He would also like to thank Mr. Milo Dahl and Mr. Robert Owens for the considerable technical assistance and useful suggestions in the experimental phase of the research they provided. The assistance of Dr. David Roth during the development of the theoretical model is also greatly appreciated. He is also indebted to Mr. Greg Henderson, who programmed the database system that was employed in generating and presenting the theoretical model results, for the fine software support.

This research was funded by the National Aeronautics and Space Administration at the Langley Research Center. Their financial support was greatly appreciated.

CHAPTER 1

INTRODUCTION AND PURPOSE OF RESEARCH

During the 1970's it was determined that methods used to predict noise levels received from jet aircraft based on linear acoustic theory badly under-predicted the spectrum levels in the frequency range of 4-10 kilohertz (kHz) for aircraft that emit high intensity acoustic levels (in the range of 120-165 decibels (dB) re 20 μPascals (μPa)). The data from which this was observed were obtained from recordings made in the very far field of the source from flyover tests [1]. Among the explanations of why the high frequency energy components of the jet noise spectrum is under-predicted is the source directional characteristics. Also, one might consider frequency dependent attenuation coefficients used in the computational procedure. However, when the directionality of the source is accounted for, and the attenuation coefficients are chosen correctly, the linear acoustic prediction techniques still predict lower high frequency content than has been observed [2].

Because of this failure of linear acoustics to predict the spectrum levels received from high intensity sources it is believed that the high frequency anomalies observed are due to nonlinear effects. A purely sinusoidal wave which is subjected to nonlinear propagation will develop into a saw-tooth or acoustic shock wave, thus shifting energy from the fundamental sinusoid to higher harmonics [3]. Likewise, this nonlinear effect will cause the intense low frequency components of the jet noise spectrum to transfer their energy to the higher frequencies. The resulting buildup of high frequency energy would then account for anomalies previously mentioned.

Previous research in nonlinear propagation of broadband noise has shown spectral distortion for plane wave and spherical wave propagation [4]. Formation of acoustic shock waves has been seen in plane waves, but not spherical waves [5,6].

In a study conducted in a plane wave tube Pernet and Payne [7] found that, for a narrow band of high intensity random noise, harmonics were generated that were similar in nature to those generated by pure tones. A spectral distortion equation that represented the generation of the high frequency harmonics as a square law process was found to be a valid approximation of this process. Webster and Blackstock [8], in another plane wave study, observed shock formation for noise with a broad bandwidth. They noted that the energy in the mid frequency range shifted to each end of the spectrum, however, the predominant shift was towards the higher frequencies. This shift of energy caused a distinct change in the slope of the spectrum.

Webster and Blackstock performed another study in which the high intensity source was in the free field [9], thus the waves were spherically diverging. The source level in this work was in the range of 120 - 145 dB. Again they observed that the energy shift was primarily from the mid band frequencies to the high band. It was also noted that the distortion process was apparent both in the near and far fields. In another publication reporting on this work [10] the results of a computer simulation of nonlinear noise propagation are presented. This simulation uses power spectrum data obtained from flyover tests to produce "statistically equivalent" waveforms. These waveforms are then operated on in the time domain in order to predict the distortion. The model was found to agree well with plane wave data; however agreement with the flyover data was not good.

The purpose of this research is to determine the degree of spectral distortion that occurs in spherically diverging high intensity noise, and to determine if the spectral distortion is an acoustic effect. To meet these objectives high intensity noise signals were captured in a free field environment at a number of locations along the propagation path. The source is an air driven transducer; thus any effect of the combustion or aerodynamics associated with a jet engine is removed. By capturing waveforms at two points in the propagation path, a direct indication of the amount of distortion is obtained. In addition to observing distortion effects a model based on nonlinear acoustic theory is used to demonstrate that the distortion effects observed are due to acoustic nonlinear distortion.

In this research study the source is an electro-pneumatic transducer capable of generating acoustic sound pressure levels (SPL's) in the range of 140-160 dB with less than 10 percent total harmonic distortion [11]. These levels are on the order of 10 to 15 dB higher than those recorded in previous research. At these high levels strong nonlinear distortion effects were observed.

The data were collected using a system consisting of a Commodore personal computer interfaced with a Nicolet 660A Fast Fourier Transform (FFT) analyzer and a Keithley digital voltmeter (DVM). Two microphones were used to acquire time and frequency domain data. One microphone was attached to a rigid support located .25 meters from the transducer outlet. The second microphone was on a computer-controlled two-axis positioning system which enabled the microphone to move to on-axis locations of .5 to 1.75 meters from the source exit, and angles up to 30 degrees off axis.

The data acquisition system and experiment are described in detail in the following chapter. In Chapter 3, results of the experiment are presented. In

Chapter 4, the experimental results are compared to waveforms that were predicted using a computer model previously developed at PSU. Also, the model's theory is discussed in Chapter 4. The last chapter provides conclusions.

CHAPTER 2

EXPERIMENTAL DESIGN

Introduction

In this chapter the high intensity source, the data acquisition system, and the experiment to observe nonlinear effects in noise are described. The Ling EPT-200 was installed in the N.C.L. anechoic chamber on a sturdy support structure as shown in Figure 2.1. A horn of exponentially increasing cross sectional area was mounted on the EPT-200 to provide better coupling to the acoustic medium.

The transducer has a high air mass flow rate and thus the air reservoir was quickly exhausted, making operational periods short (on the order of 3 to 6 minutes). A personal computer was used to control the data acquisition in order to obtain data in the short operational periods. The computer controlled all phases of the data acquisition, which included microphone positioning, air supply pressure monitoring, control of a Fast Fourier Transform analyzer and other instrumentation, and data storage. The data acquisition system is explained in detail later in this chapter.

The objective of the experiment was to observe wave distortion over different propagation distances. Two microphones were used–one stationary and near the source, the other on a traversing mechanism which was controlled by the computer. The computer measured the propagation delay between the microphones and set the spectrum analyzer to delay the capture of the waveforms between the input channels. Using this technique we were able to record the same waveforms at two different points in space and directly observe the nonlinear effects.

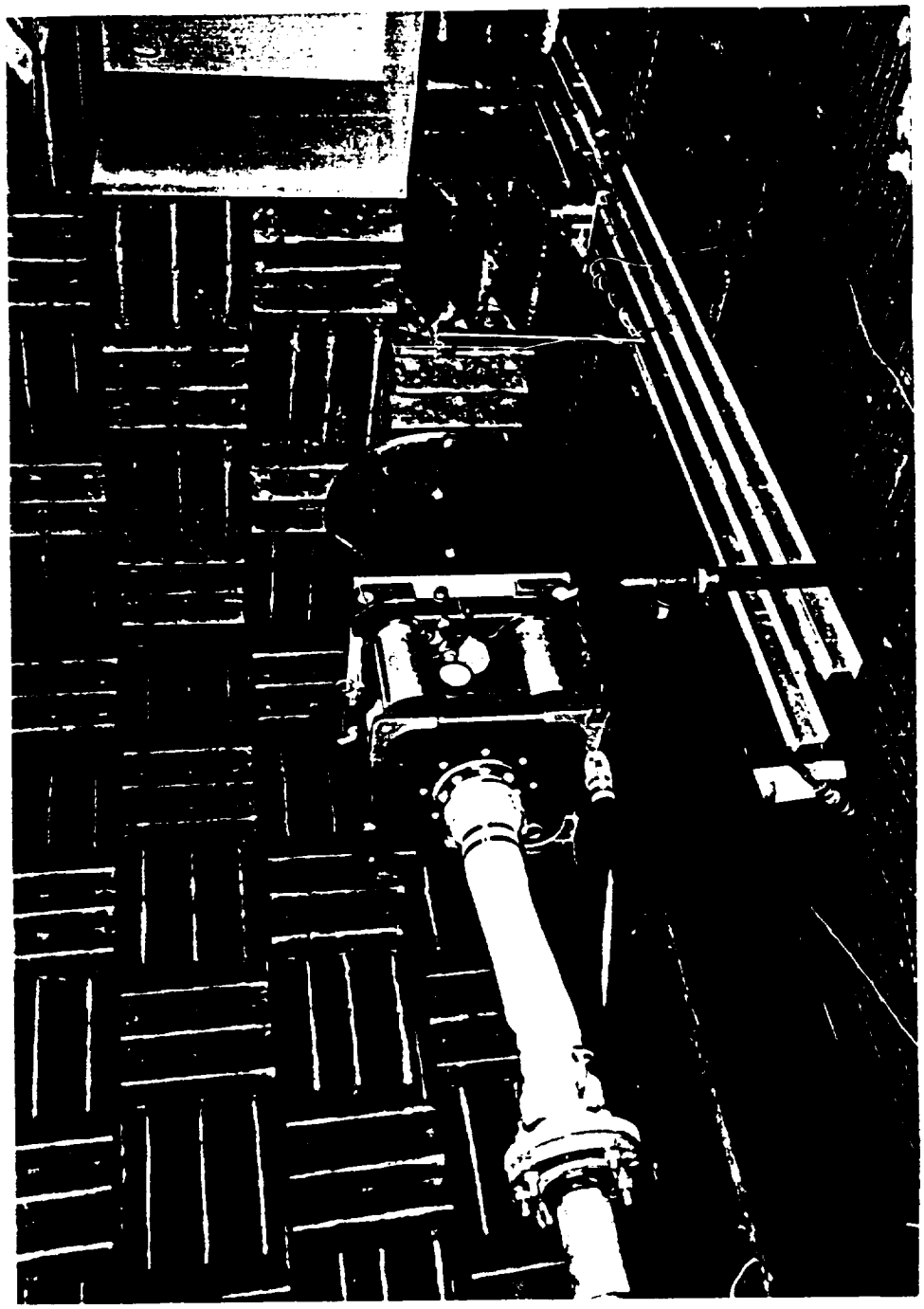

Figure 2.1 Ling High Intensity Source in Anechoic Chamber

The High Intensity Source and the Anechoic Chamber

The Ling EPT-200 high intensity source is an electronically controlled air valve capable of generating 10 Kilowatts of acoustic power. It is able to reproduce any complex waveform within its operating frequency range of 20 to 1250 Hz. The transducer is powered by a 3.5 KW power amplifier which is coupled to a magnetic field supply. The magnetic field opens and closes the valve according the electrical input waveform. The throttled air passing through the valve produces the acoustic waveform. The transducer and power supply are sold as a unit by the manufacturer. An exponential horn was coupled to the transducer to provide for efficient acoustic power transfer.

The air supply system was located in the Aerospace Engineering Laboratory. It can provide a 2000 cubic foot reservoir of air at a constant pressure of 150 PSIG. The system was designed to provide up to 4000 SCFM of air and is regulated through a 2.5 inch Leslie regulator. The Leslie regulator was found to react too sluggishly to the rapidly changing demands of the Ling transducer; thus it was bypassed. Control of the air supply was reduced to opening a gate valve to supply the desired back pressure. The air reservoir was then blown down until the transducer could no longer achieve the desired acoustic level. At this point the experiment was halted until the air reservoir was refilled.

The input signal to the amplifier was supplied by a General Radio 1/3 white noise generator. The wide band noise output by this generator was filtered using a General Radio octave band multifilter. Shown in Figure 2.2 is the spectrum of the filtered noise input to a pre-amplifier which was then sent to the Ling power amplifier. The spectral weighting used was chosen to resemble the spectra of loud jets.

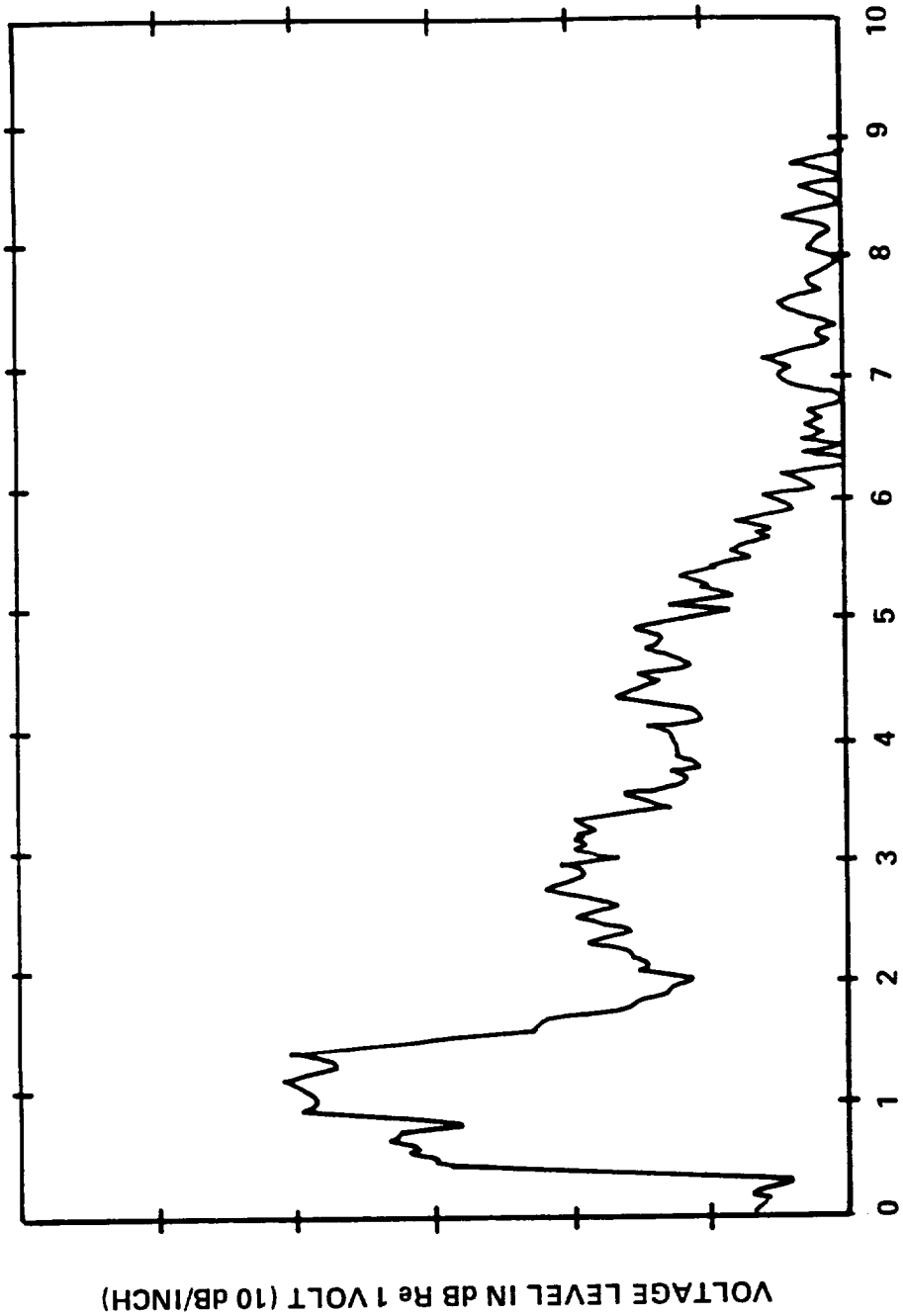

Figure 2.2 Typical Input Signal Spectrum

The NCL's anechoic chamber usable space (the space inside the wedge tips) is 14 ft by 17 ft by 9 ft. The low cutoff frequency for the chamber is 125 Hz. The transducer when operating at, or near, full capacity exhausts over 1000 SCFM of air to the chamber. In order to vent this air to the atmosphere an airflow eductor designed for the chamber was installed. The eductor is designed to exhaust 4000 SCFM of air to the outside of the building with a maximum backpressure of 1 inch of water. Previous research indicated that the eductor does not significantly alter the anechoic chamber's free field environment [12].

Data Acquisition System

The data acquisition system was designed to capture the acoustic waveforms at different points along the propagation path. The system can be divided into two sections, the analog signal capture and processing section and the digital signal capture processing, and storage. The analog system consists of the microphones, pre-amplifiers, and amplifiers. At the point where the microphone signals are input to the spectrum analyzer, the digital system begins. The digital system consists of the microcomputer, it's floppy disk unit, and the spectrum analyzer. Other devices were utilized in the system for experiment control and monitoring. Figure 2.3 is a block diagram of the overall system.

The microphones used were Bruel & Kjaer condenser microphones, one 1/4 inch and the other 1/8 inch diameter. These microphones have a flat frequency response ($\pm$ 2 dB) in the range of 3 Hz. to 70 kHz. The upper limit of their dynamic range is 180 dB ($<$ % 10 distortion). The 1/8 inch microphone was fixed on a rigid support located 1/4 meter from the exit of the transducer's horn. The microphone was positioned at this point to minimize the effects of the air turbulence at the transducer exit, while remaining close enough to capture the

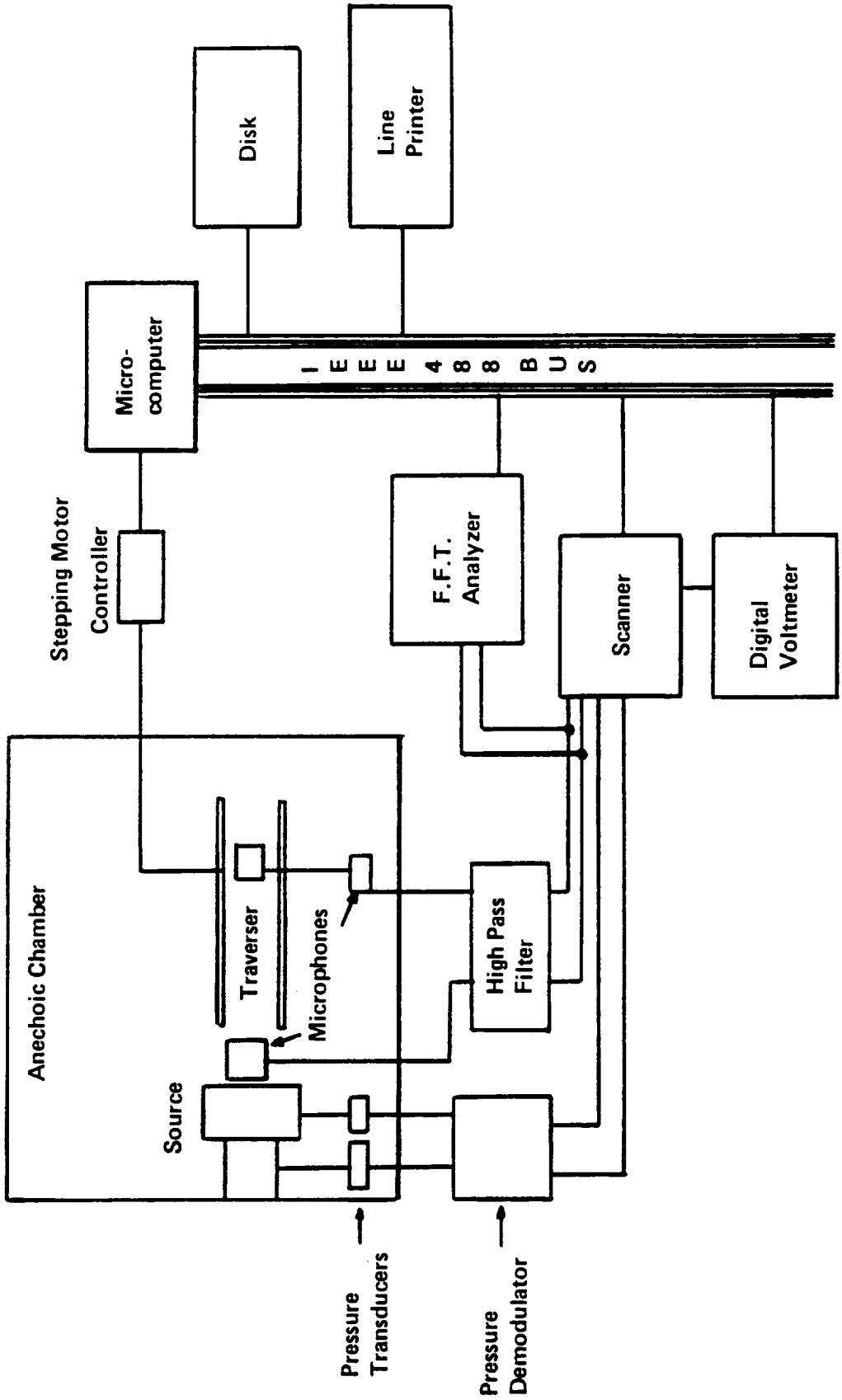

Figure 2.3 Block Diagram of Nonlinear Noise Propagation Experiment

waveforms early in the propagation path. The 1/4 inch microphone was mounted on turntable which was mounted on a linear traversing table, shown in Figure 2.4.

At the high intensity levels generated by the source, the microphone output voltage would overload the input attenuators of the spectrum analyzer. The microphone signals were pre-amplified to supply the analyzer with signals which were within its operating range. Normally, the pre-amps, Hewlett Packard voltmeters, were operated as attenuators of -10 to -20 dB. The frequency response of the voltmeters is flat to 500 kHz, much beyond the analysis range.

The microcomputer used to control the experiment was a Commodore 4032. It has a Motorola 6502 microprocessor as its main processor, 32 Kilobytes of Random Access Memory (RAM) for program and data storage and a resident operating system which runs an interactive version of the BASIC programming language. The operating system also allows for programming in the machine language. An editor/assembler was purchased to aid in the development of assembly language programs. The Commodore 4032 has four Input/Output ports. Two of the ports service cassette tape decks which store programs and data. The other ports are 8 bit parallel bidirectional ports. One of these ports supports the IEEE-488 bus standards while the other may be programmed by the user to support nonstandard instrumentation. The IEEE-488 bus standard allows the computer to communicate with as many as 15 devices on one set of 24 parallel lines.

Three instruments and a Commodore 4040 Dual Drive Floppy Disk were controlled through the IEEE-488 port. The disk drive was used for data and program storage. It has a Motorola 6504 as a central processor that executes its resident disk operating system. With two drives it has a storage capacity of 349.7

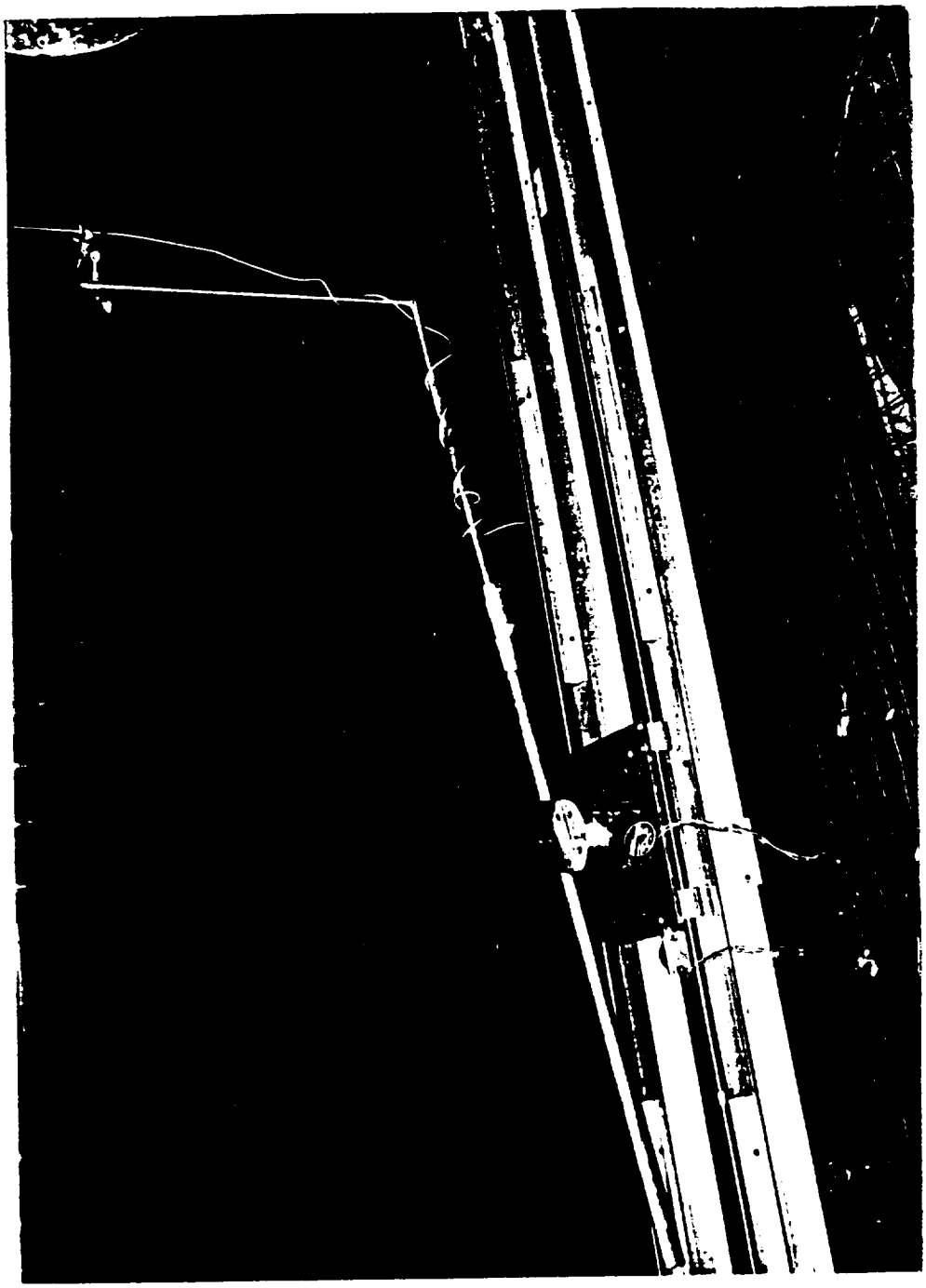

Figure 2.4 Microphone Positioning System

kilobytes. Also residing on the IEEE bus are the data acquisition instruments, a Keithley Model 702 Scanner, a Keithley Model 192 Digital Multimeter (DMM), and a Nicolet 660A Dual Channel Fast Fourier Transform Spectrum Analyzer (660A). The 660A was interfaced to the IEEE-488 bus through a TNW 2000 Serial Interface Module. This device allowed for more reliable communication between the computer and the 660A. The computer and all devices are shown in Figure 2.5. The user programmable port was used to command the Slo-Syn motor translator module, which then drove the stepping motors. The complete system is a rather inexpensive and powerful acoustic data acquisition system.

Experimental Procedures

The acquisition system described above provided the opportunity to collect quality data. The computer control provides speed when interfaced to the spectrum analyzer. At the same time the pressure monitoring system enabled the operator to maintain a constant air pressure to the source. In this section, the procedures employed to acquire the data are described. These include calibration techniques of the transducers and the computer control program validation and operation.

Microphone calibration voltages and pressure transducer calibration were performed each time the experiment was run. Also before any data were acquired, the microphone position was set to a known location. The calibration constants were measured using the same data acquisition system as was run during the experiment.

A simple program written in BASIC was used to control the microphone calibration procedure. A B & K type 4220 pistonphone calibrator was used in the calibration of the microphones. This device emits a known sound pressure level of 124 dB at 250 Hz. The program instructs the operator to place the calibrator

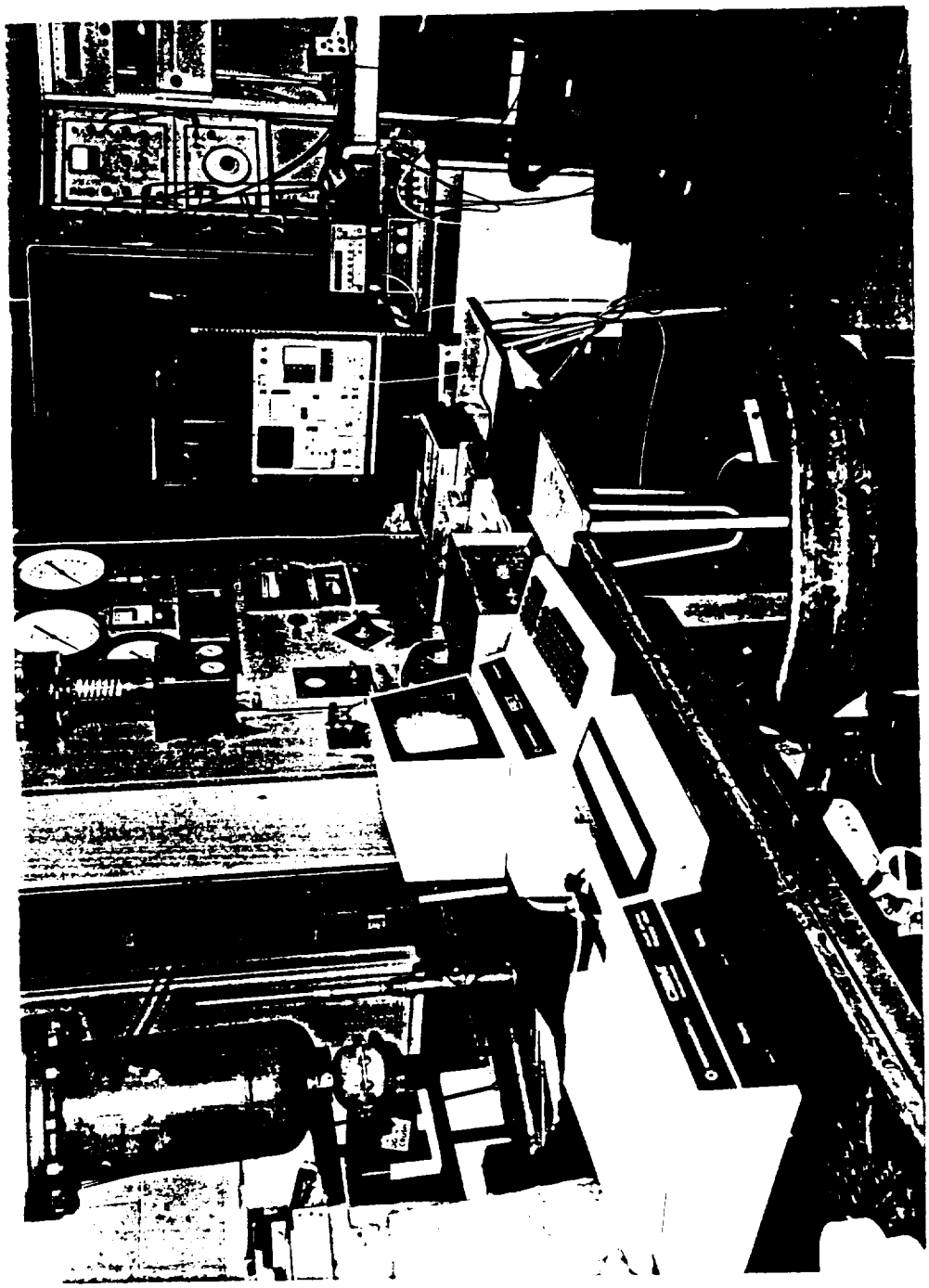

Figure 2.5 Data Acquisition and Control System

on a microphone. After a waiting period to allow the operator time to get the calibrator in place the output voltage is measured on the DMM recorded, and printed on the line printer. This provides a permanent record of the calibration voltage as well as a signal to the operator that the procedure has been completed. Any gain factors applied are also recorded by the calibration program.

The pressure transducers were Validyne DP15 variable reluctance type transducers which convert a pressure signal to an electrical signal. A signal carrier demodulation unit made by Validyne was used to achieve a D.C. voltage which was read by the DMM. The pressure transducer's sensitivities can be adjusted using the carrier demodulator units potentiometers. Calibration of the transducers consisted of first, zeroing the transducer, and second, adjusting the carrier-demodulator to achieve the desired slope of the calibration. To zero the transducers both sides are exposed to atmosphere, and the carrier demodulator was adjusted to arrive at zero volts output for this condition (corresponding to zero PSI differential). The desired slope of the calibration curve was 10 PSI/volt. To obtain this, the transducer was next exposed to 10 PSIG and the carrier- demodulator was adjusted to achieve an output voltage of 1 volt. This procedure was repeated for 20 and 30 PSIG. This procedure is a two pass operation, having gone through it once the second pass is necessary to check the zero and fine tune the calibration.

Calibration of the microphone positioning consisted of two phases. The first phase was necessary to check the software which drove the motors. This consisted of marking where the microphone was positioned, entering a new position, and when the computer had executed the program, checking the microphone position using a tape measure. Once the program was seen to operate correctly this procedure was never repeated. The second phase of the positioning calibration

consisted of placing the microphone in a marked location at the beginning of each test run. This was achieved using the stepping motor translator in a manual mode in which the stepping pulses are generated internally. Placing the microphone in the same location at the beginning of each run ensures that the positioning is accurate.

The experimental control program allowed for operator control and intervention. The program accepted as inputs from the operator the trigger level (in decibels) and the microphone position. The operator was also able to accept or reject data for permanent storage. While allowing the operator to define operating parameters, the program controlled all the devices once the experiment was running.

The program has three major segments, the initialization phase, the data acquisition phase, and the microphone positioning phase. The user can choose between these different phases from a menu. This allowed the user to choose the experimental sequence of operations during run time. The program normally displays the menu until the user has chosen the phase which is to be operating.

The initialization phase executes automatically every time the program is restarted. If all the necessary inputs are typed in correctly, this phase need not be executed again. However, if an error did occur during the initialization, or one was suspected, the initialization phase could be called from the menu to check and/or change an input parameter.

The microphone positioning phase of the program required as inputs the desired angular and axial displacement of the microphone. It calculated the number of steps needed to move the microphone from its present location to the desired one, and pulsed the motor translator accordingly.

The program spent much of the time in the data acquisition phase. The acquisition phase operated in two capture modes, the time history mode and the spectral mode.

The program, when working in the time history mode of operation, was designed to capture the same waveforms from each microphone. In order to do this first the time delay needed for the acoustic wave to travel the distance between the microphones must be determined and set on the spectrum analyzer.

A first attempt at determining the delay was to measure the temperature of the air in the chamber using an integrated circuit temperature sensor, an LM 335. This sensor outputs a DC voltage which is proportional to the temperature. After measuring the temperature, the computer calculated the speed of sound, and knowing the spacing between the microphones, a delay time was calculated. This approach produced results in which portions of the same waveforms were captured at each microphone location. Another technique was found which utilized the spectrum analyzer in the correlation mode, and the cross correlation function. This technique measures the time delay between the two microphones directly and provided excellent results.

The correlation function of two sets of random data describes the dependence of the values of one set of data on the other, and will yield time delay information of a system directly. As the output from the system is displaced in time relative to the input, the cross-correlation function will peak at that time displacement equal to the time required for the signal to pass through the system. Using the cross-correlation technique we were able to very accurately determine the propagation delay between the microphones and capture waveforms at two points

on the propagation path. Figure 2.6 shows a typical cross-correlogram for the experimental setup.

Having determined the propagation delay time, the program goes into the acquisition phase. During this phase, the SPL at the two microphone locations and two pressures along the transducer input are measured and displayed to the screen. The signals from these transducers were switched using the scanner and read by the DMM. From the input voltages, the air supply pressure and the sound pressure levels were calculated using the calibration constants input to the program and the equations shown below:

$$SPL = 20 * \log(V_m/V_{cal}) + 124 - GAIN$$

$$Pressure = 10 * V_m$$

where V_m is the voltage measured, V_{cal} is the calibration voltage measured for each microphone, GAIN is the external gain due to the signal amplification. The constant 124 is the known SPL for the calibration voltage, and 10 in the pressure equation is the sensitivity the pressure transducer (in PSI/VOLT).

When the SPL measured at the near microphone was above the trigger level the spectrum analyzer was triggered, and thus the waveform captured. The waveforms are displayed on the video screen of the spectrum analyzer and the user then had the option to transfer the waveform data to the computer for permanent storage, or to reject them. If it was decided to save the data they were transferred in a compact three byte format to the computer, and then stored to disk. Data transfer from the spectrum analyzer consisted of dumping the memory buffers of the analyzer to retrieve the data and dumping of a memory buffer which stored the analyzer's current operating conditions. All communication between the analyzer and the computer were controlled by machine language subroutines to decrease the time spent transferring data. Having stored the data, the program

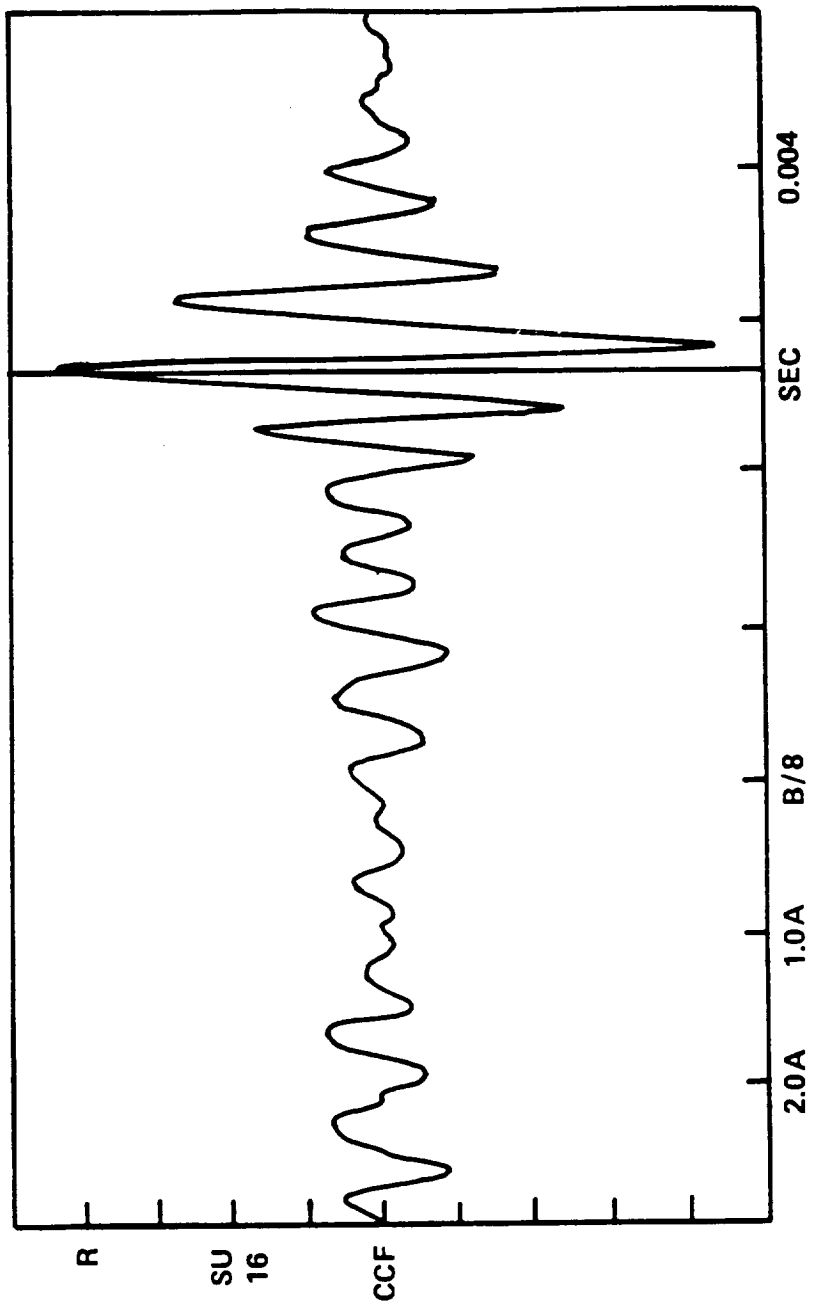

Figure 2.6 Typical Cross Correlation Function

returned to the main menu. If the data were rejected the computer goes back to scanning the microphone and pressure inputs until the trigger level is again exceeded.

In the spectral mode, the computer again positioned the microphone, monitored the SPL at the transducer exit and commanded the spectrum analyzer to capture the data when the level exceeded the trigger level. Again, the user could choose to reject the data, and the computer would continue the experimental monitoring. If the data were accepted four memory buffers which contain the spectral information plus the buffer which contained the analyzer's current operating status were transferred and saved. Data were stored on the 4040 disk in the same compact three byte format as the time history data.

Data Reduction

Data reduction included converting the compact digital format in which the data were stored into voltages and converting these voltages to physical units. Time history mode data consisted of 1024 samples of the microphone output voltages equally spaced over the time window, typically 0.008 seconds. In the spectral mode, the analyzer output was the amplitude of the spectra in voltages for 400 equally spaced bins over the frequency range, typically 0-10 kHz.

The conversion of the time history data consisted of calculating the absolute voltages, and then the sound pressures. The calibration constants and external gain, the data from the buffer which contained the analyzer's setup and the normalized data were used in the conversion program. From the set up data, the time window setting and the analyzer input attenuator settings were decoded.

The sound pressures and times were then calculated using the following equations

$$T_n = n * W/1024$$

$$V_n = G_{attn} * D_n$$

$$P_n = D_n * V_{cal}$$

where n is the sample number, T_n is the time offset of the n^{th} sample in seconds, W is the spectrum analyzer's time window, V_n is the microphone output voltage, G_{attn} is the spectrum analyzer's input attenuator setting, D_n is the normalized voltage level, P_n is the sound pressure in N/m^2 , V_{cal} is the calibration voltage at 124 dB expressed in $N/m^2/volt$.

The spectral mode data were converted from the stored normalized voltages and the frequency data were generated using the equations

$$F_n = n * F_{max}/400,$$

$$V_n = G_{attn} * R * D_n$$

$$SPL_n = 20 * \log(D_n/V_{cal}) + 124 - Gain$$

where n is the bin number, F_{max} is the spectrum analyzer's frequency range setting, V_n is the output voltage of the microphone measured by the spectrum analyzer , G_{attn} is the spectrum analyzer's attenuator setting, R is a relative factor based on the window setting of the analyzer, and D_n is normalized voltage level. The frequency range setting, attenuator settings, number of samples, and weighting function setting were decoded from the stored analyzer set-up data. After the data were converted they were stored on floppy disk in the reduced form and later plotted on a Tektronix 4662 Interactive Digital Plotter. The resulting waveforms and spectral data are presented in the next chapter.

CHAPTER 3

PRESENTATION AND ANALYSIS OF RESULTS

Introduction

The measured data are presented in this chapter. Both the time history data and spectral data are presented.

Data were collected with microphone separation distances in the range of 0.15 meters to 2.0 meters. In all cases, the near microphone was located 0.25 meters from the exit of the source. The second microphone's position varied. Trigger levels were chosen at 140, 150, and 160 dB in order to observe waveform distortion at different levels of nonlinearity. The data clearly demonstrate that waveform distortion is occurring at these levels. On-axis data are presented for many locations while off-axis data are presented for only a few.

Time History Data

Due to the enormous difference between the maxima of the two recorded sound pressure waves, which range from 1000 to 15000 N/M^2, the data has been normalized. Each pressure waveform was normalized to the maximum pressure of the waveform. The normalization makes the overlay plots presented show the wave distortion more clearly. This technique does, however, tend to exaggerate waveform transitions from the positive to negative values. The normalization factor is noted on each plot in the lower left hand corner. The distance of the traversing microphone from the noise source is listed in the lower right hand corner.

Waveforms for signals in the range of 140 to 150 dB are shown in Figures 3.1 and 3.2. Figure 3.1 shows distortion occurring at a distance of 1.2 meters. The waveform is steepening faster at the higher frequency segments more than

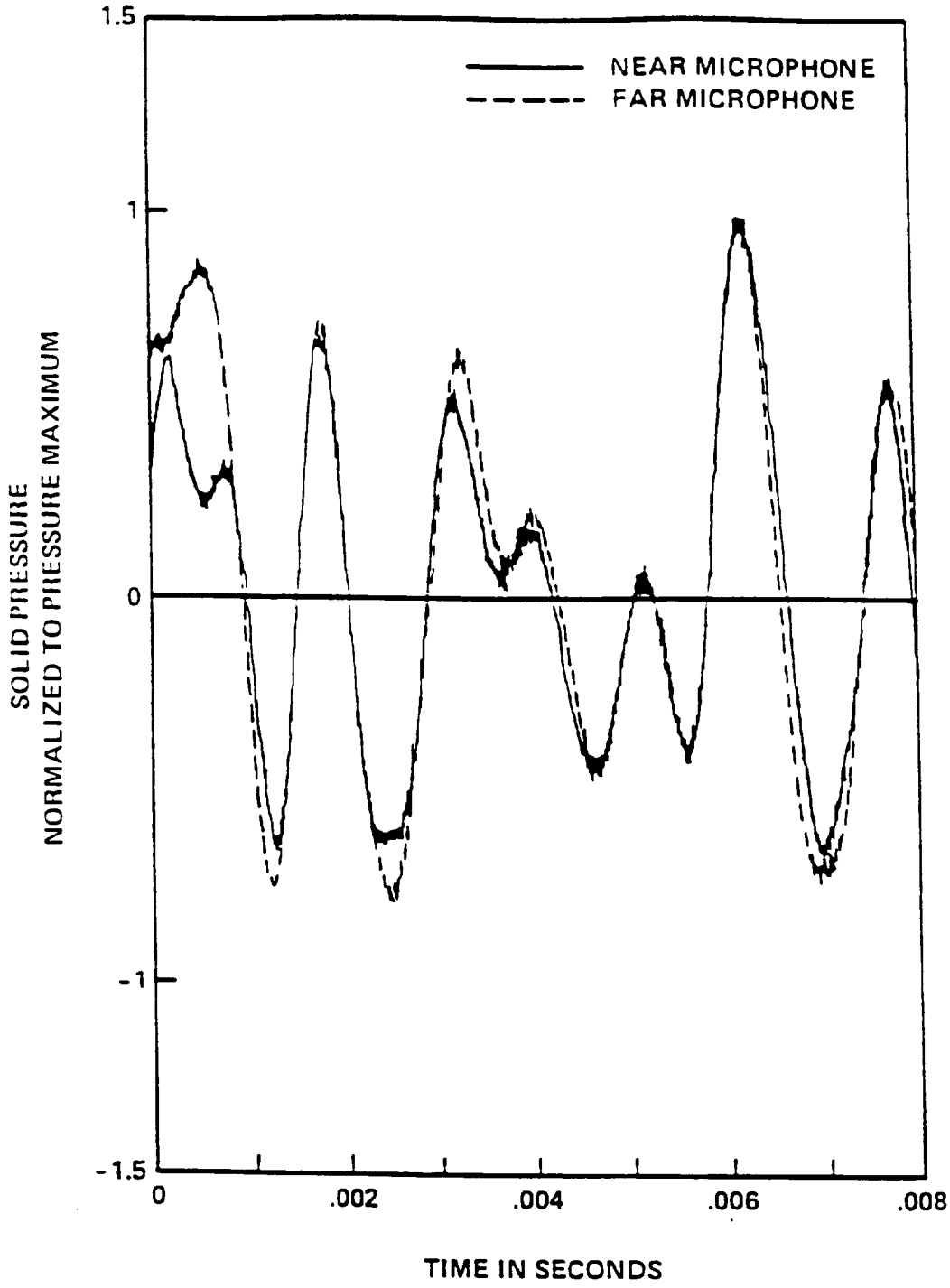

NEAR MIC NORMALIZED BY 544.5 N/M12
FAR MIC NORMALIZED BY 183.7 N/M12 ON AXIS 1.2 METERS FROM SOURCE

Figure 3.1 Low Level Distortion, Near Microphone Peak Level 148 dB, Far Microphone Peak Level 139 dB

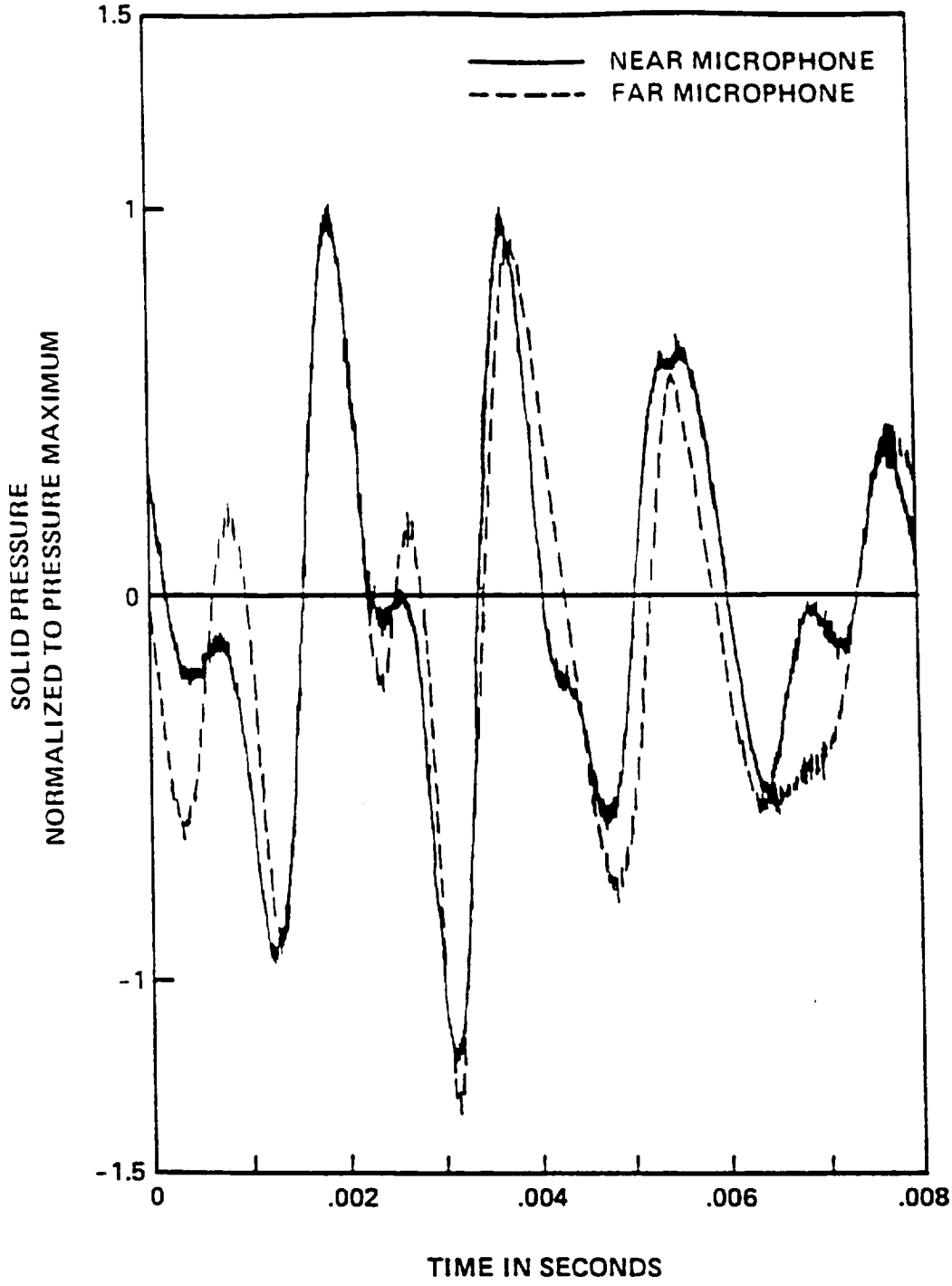

NEAR MIC NORMALIZED BY 474.01 N/M12
FAR MIC NORMALIZED BY 123.9 N/M12 ON AXIS 1.6 METERS FROM SOURCE

Figure 3.2 Low Level Distortion, Near Microphone Peak Level 147 dB, Far Microphone Peak Level 135 dB

others. At a longer propagation distance and a lower input level, the wave distortion becomes more apparent as shown in Figure 3.2. Again the higher frequency segments show more distortion.

At levels of 150-160 dB, the distortion grows at a much faster rate. Figure 3.3 shows that in a short distance the distortion occurs for all frequencies in the waveform. In another half meter some waveform crests are already approaching shocks (Figure 3.4). Again, the high frequency components are cresting at a faster rate than the lower frequency components. This waveform also shows the dependence of the distortion rate on the amplitude of the peaks and troughs of the waveform. The fourth peak (looking left to right) is approximately the same frequency as the next, yet it shows much less steepening due to the lower amplitude. Figure 3.5 shows a waveform of higher peak levels still further down the propagation path. Again the distortion is seen to be dependent on both frequency and levels. Far downstream, the distortion is becoming noticeable for all the crests of the waveforms. By this point the propagated waveform's shape is much different than the baseline waveform shape.

At levels of 160 dB and greater, the distortion process is greatly accelerated. Figure 3.6 shows a waveform with a peak amplitude of 167 dB. At this intensity, the waveform distortion is apparent in the near microphone data. The other microphone is 0.4 meters from the near microphone. The distortion in the short distance (0.15 meters) between the microphones is small, but distinguishable. Although the waveform at the first microphone is approaching a stable sawtooth, the distortion continues as seen in Figure 3.7. Both waveforms show very high frequency energy. The components of the energy at higher amplitude however have already become shocks at the near microphone location, yet the lower energy components continue distorting and have almost reached shock 1 meter from the

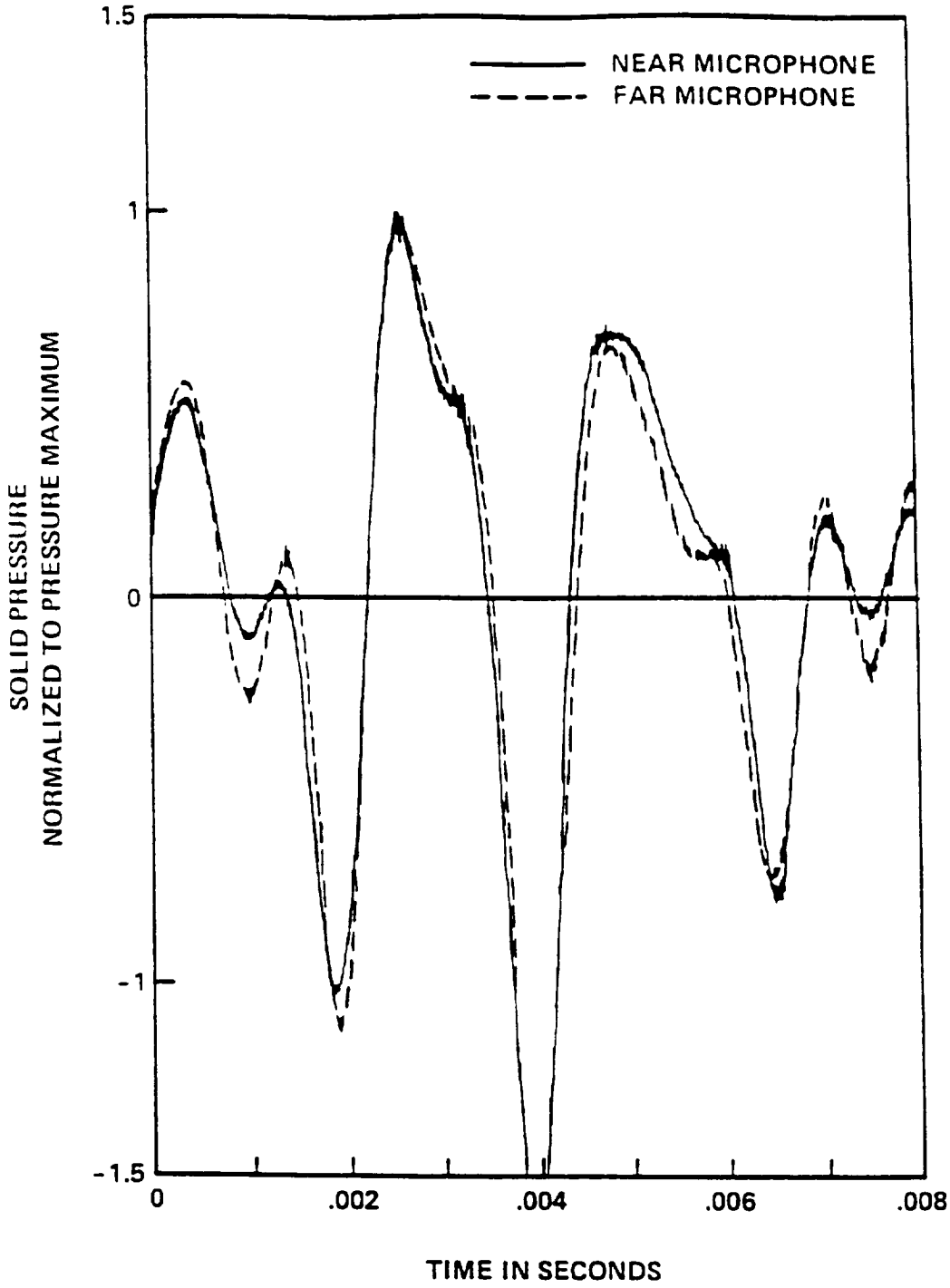

NEAR MIC NORMALIZED BY 1151.17 N/M12
FAR MIC NORMALIZED BY 1012.32 N/M12 ON AXIS .4 METERS FROM SOURCE

Figure 3.3 Medium Level Distortion, Near Microphone Peak Level 155 dB, Far Microphone Peak Level 154 dB

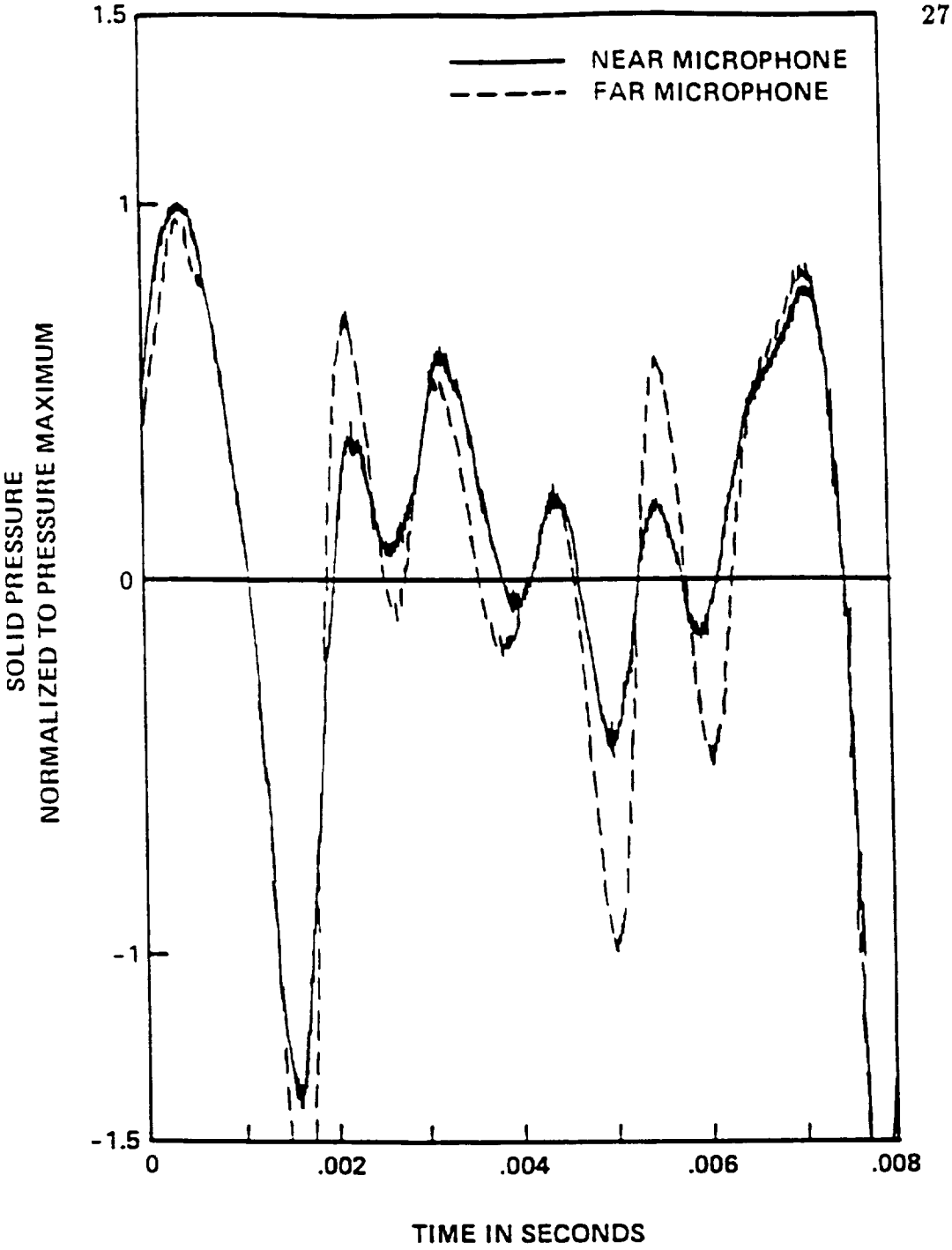

NEAR MIC NORMALIZED BY 1057.2 N/Mt2
FAR MIC NORMALIZED BY 364.28 N/Mt2 ON AXIS .9 METERS FROM SOURCE

Figure 3.4 Medium Level Distortion, Near Microphone Peak Level 154 dB, Far Microphone Peak Level 145 dB

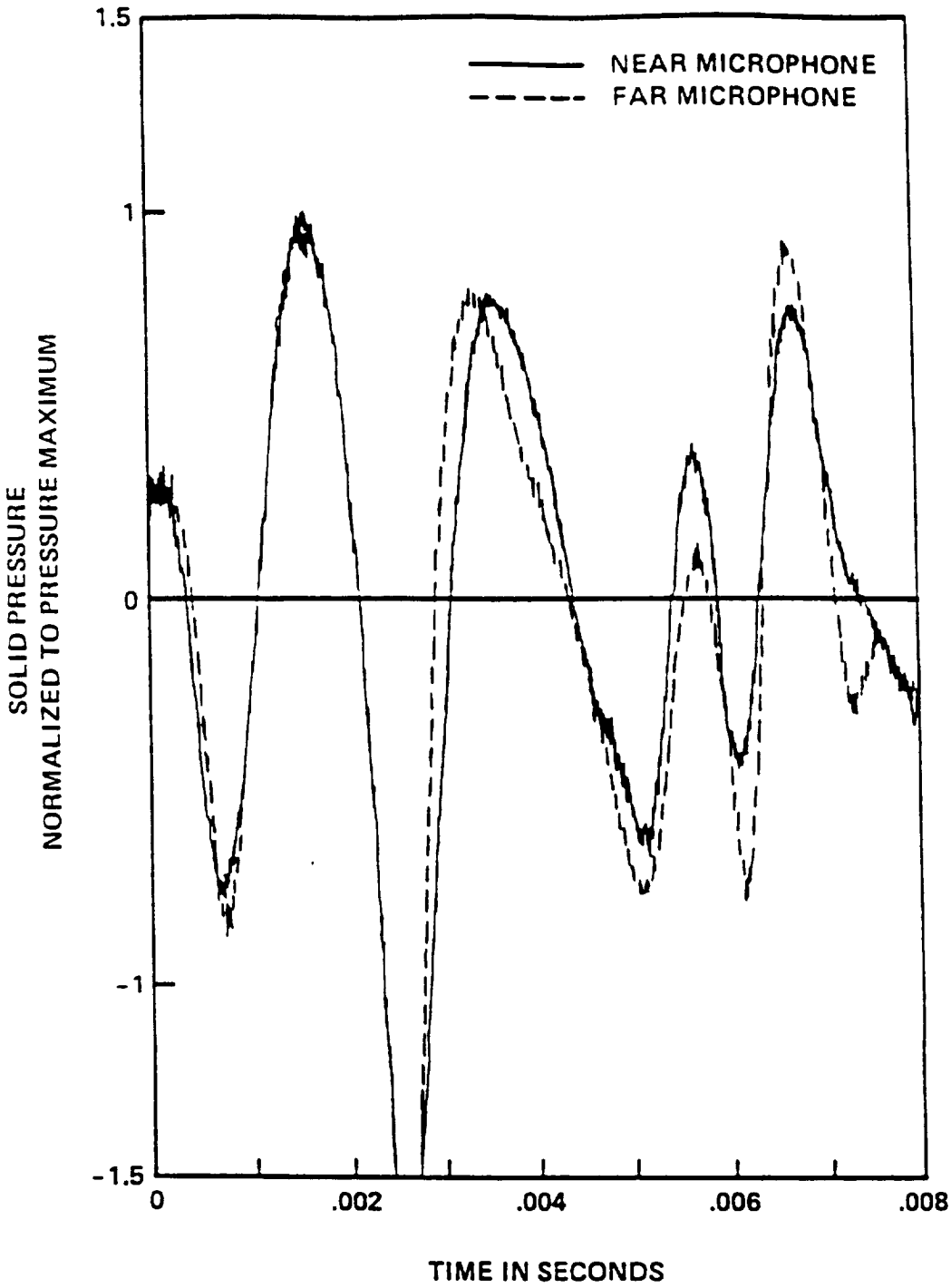

NEAR MIC NORMALIZED BY 1634.16 N/M12
FAR MIC NORMALIZED BY 504.2 N/M12 ON AXIS 1.2 METERS FROM SOURCE

Figure 3.5 Medium Level Distortion, Near Microphone Peak Level 158 dB, Far Microphone Peak Level 139 dB

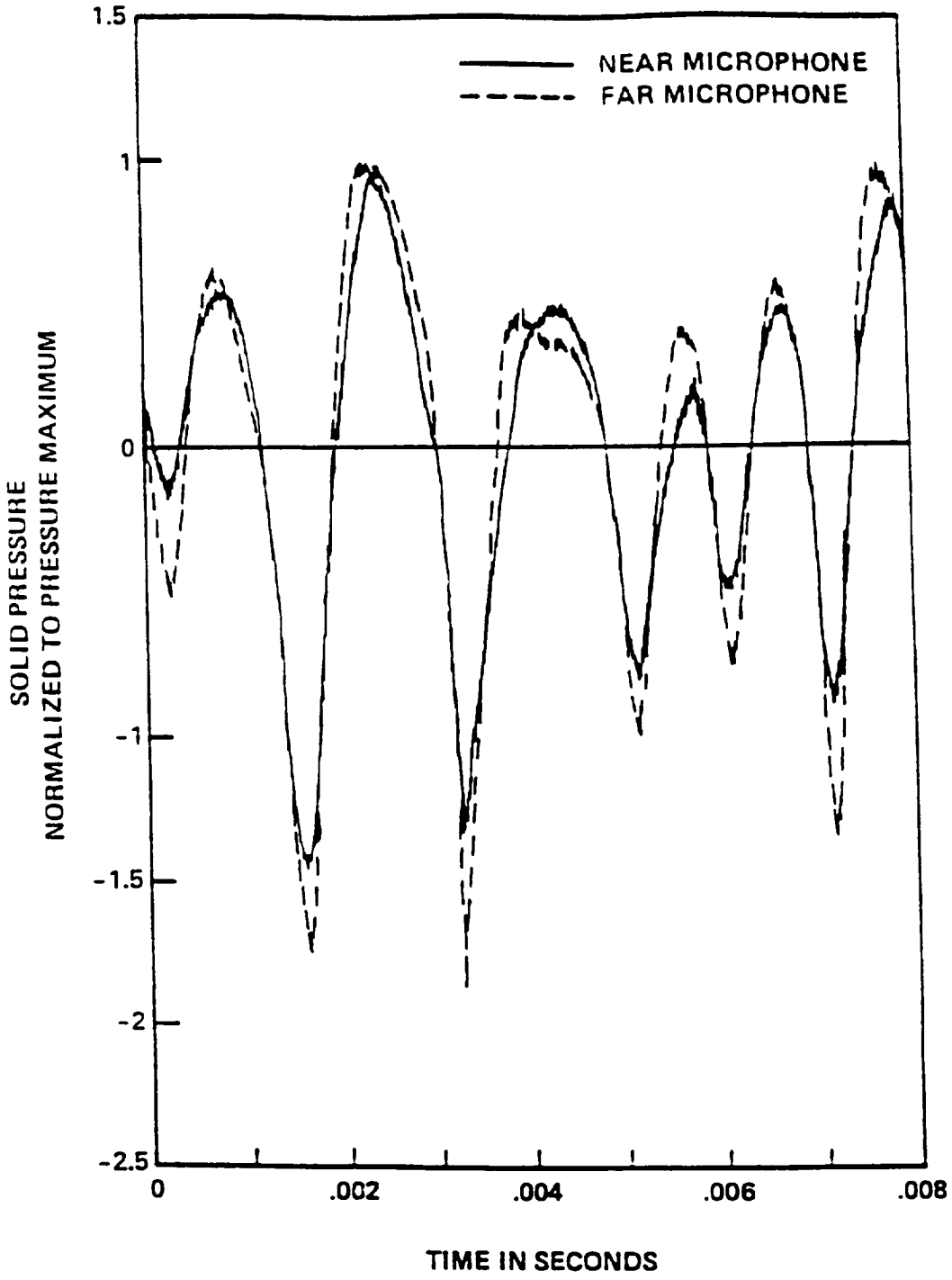

NEAR MIC NORMALIZED BY 4486.55 N/M12
FAR MIC NORMALIZED BY 3722.16 N/M12 ON AXIS .4 METERS FROM SOURCE

Figure 3.6 High Level Distortion, Near Microphone Peak Level 167 dB, Far Microphone Peak Level 165 dB

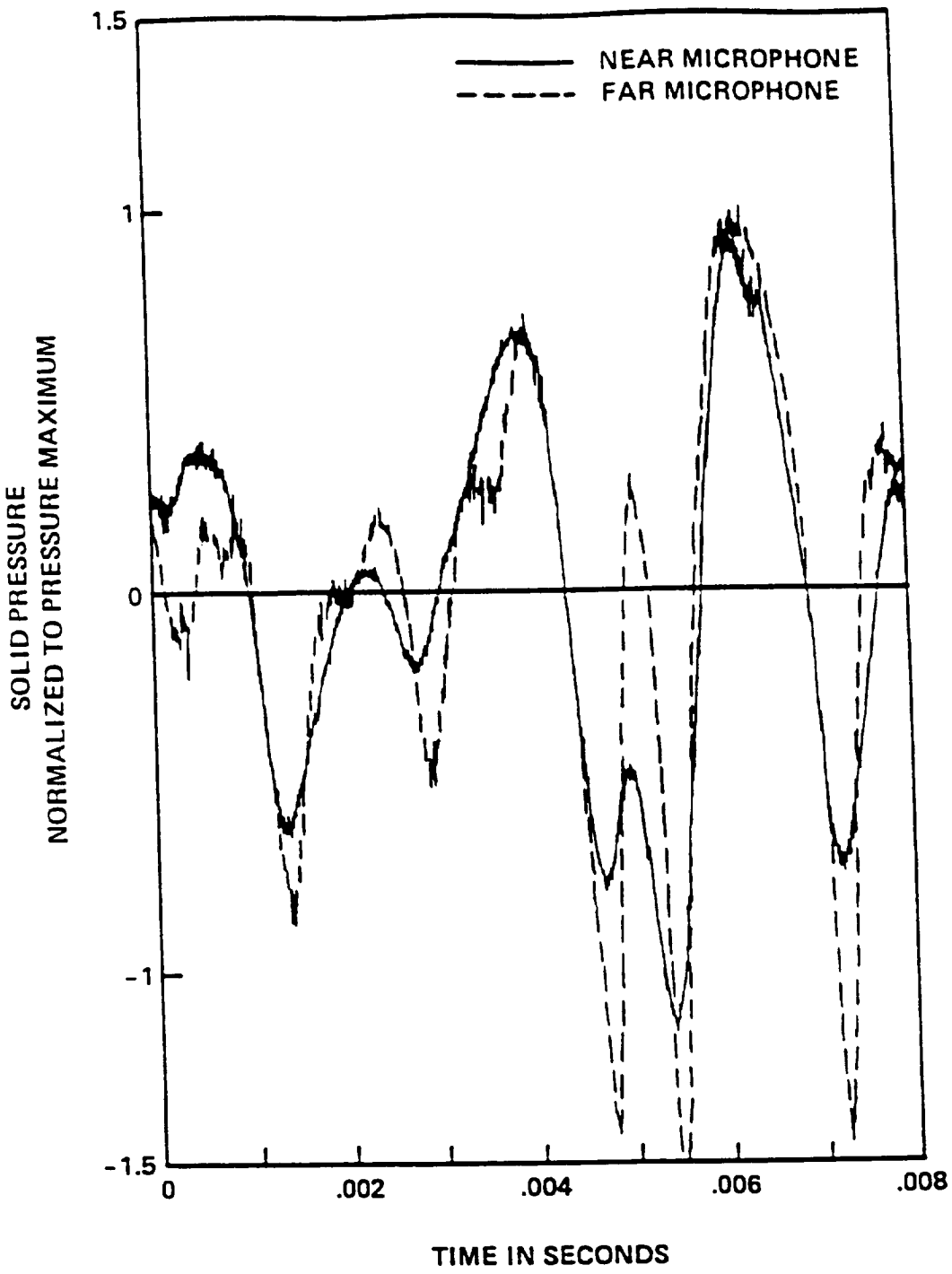

NEAR MIC NORMALIZED BY 3409.23 N/M12
FAR MIC NORMALIZED BY 484.85 N/M12 ON AXIS 2.1 METERS FROM SOURCE

Figure 3.8 High Level Distortion, Near Microphone Peak Level 164 dB, Far Microphone Peak Level 147 dB

source. Figure 3.8 shows the distortion over 2.1 meters of propagation. Once again, the high frequency energy is present in both microphone samples due to the immediate distortion at these levels. The high frequency buildup in fact is completely destroying the lower frequency components of the wave structure as can be seen in the first and third wave crests.

These data show that the nonlinear effects for narrow bandwidth noise distort the separate components of a waveform at different rates. These rates depend both on the amplitude and the frequency of the components. Even at the high intensities (> 160 dB), when the distortion is great at very short distances, this trend occurs. This will be shown in the next section where spectral data for the high intensities show the growth of high frequency energy.

Spectral Data

Spectral data were acquired using the spectrum analyzer in a summing fast Fourier transform mode. The input waveform shapes were generated by a white noise generator that was then band-passed through a spectrum shaper as explained in Chapter 2. The spectral shapes of the input signal were not changed in the testing sequence.

As seen in the time history data the high frequency buildup in the waves occurs most rapidly at intensities above 160 dB. As with the time history data, these data have been normalized to allow for direct comparison. The normalization factors for these data are their root mean square levels, and are recorded on each figure in the lower left hand corner. Channel A recorded data from the near microphone, Channel B recorded data from the traversing microphone. Figure 3.9 shows two spectra at a low level. At this level, 148 dB, the high frequency energy in both signals is well below the dynamic range of the acquisition system. Between 500 and 3000 Hz, the far spectrum does show a slight increase in level,

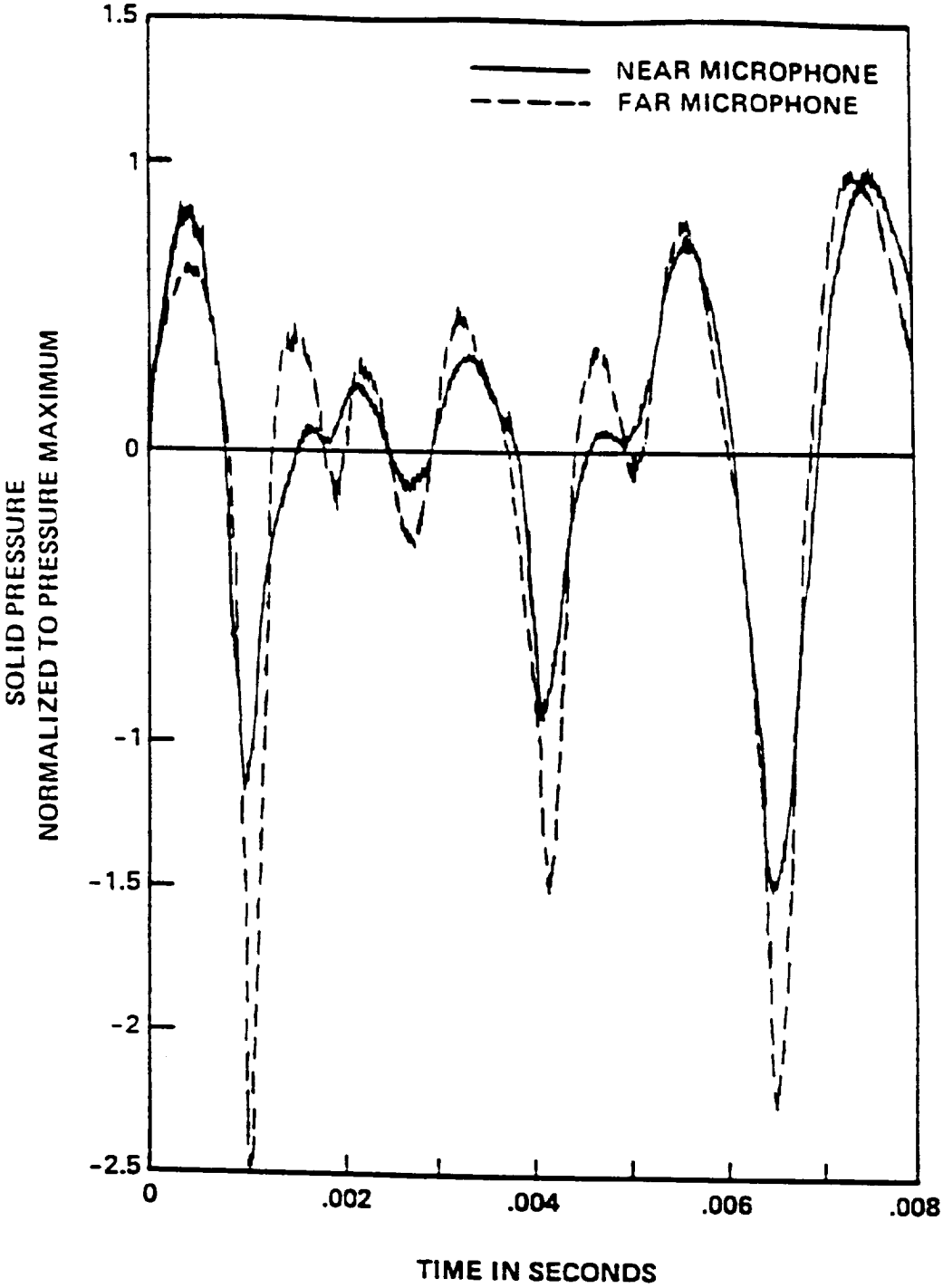

NEAR MIC NORMALIZED BY 4138.81 N/Mt2
FAR MIC NORMALIZED BY 1268.07 N/Mt2 ON AXIS 1 METER FROM SOURCE

Figure 3.7 High Level Distortion, Near Microphone Peak Level 166 dB, Far Microphone Peak Level 156 dB

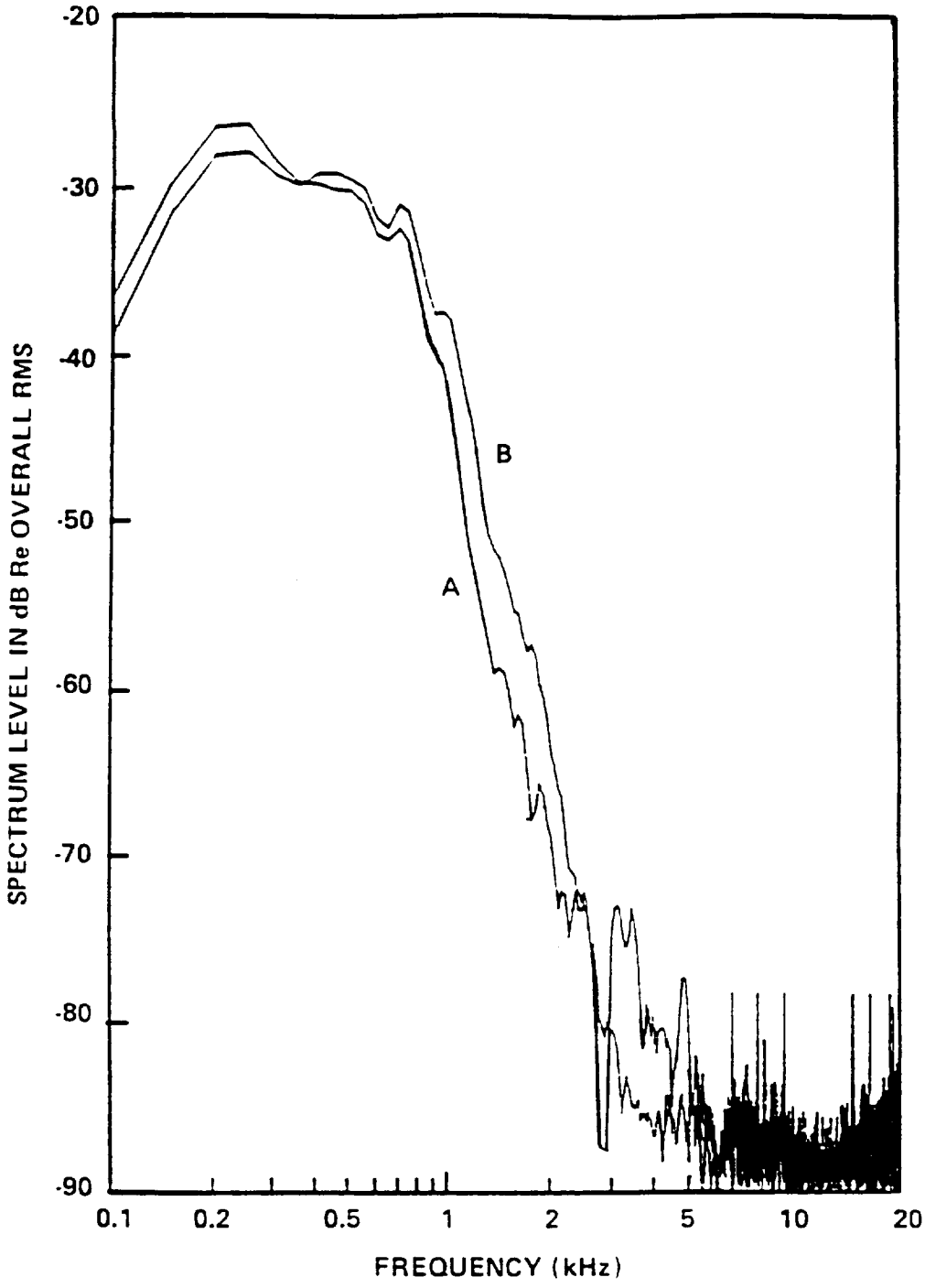

R.M.S. (A) = 147.7 dB
R.M.S. (B) = 138.1 dB

RADIUS = 1.12 METERS
ANGLE = 0 DEGREES

Figure 3.9 Spectral Data, Low Level Distortion

beyond 3000 Hz both signals fall off. Due to the low frequency levels for the lower intensity data, only high intensity data are presented here.

In Figure 3.10 the microphone separation distance is 0.15 meters. One can see the buildup in high frequency energy in the near microphone compared to Figure 3.9. The spectrum from the far microphone data shows an increase of 5 dB between 8 and 20 kHz, and a drop of 1 dB or less below 600 Hz (the spectra actually cross around 600 Hz). As the propagation distance is doubled, to where the traversing microphone is 0.8 meters from the source, the spectrum gains over 10 dB at the higher frequencies (Figure 3.11). The high frequency increase is over 5 dB from 2 kKz and beyond. The lower frequency has been diminished 3 dB in the distortion process.

Figure 3.12 shows data at 1.2 meters from the source. Again, the spectral shape is being changed as the distortion continues. The high frequency energy again has gained an extra 5 dB beyond 2 kHz, now being 10 dB above the reference. The lower frequency dropoff is still around 3 dB, thus the energy shift is predominately from the midband frequencies to the high frequencies. Figure 3.13, at 1.6 meters shows the spectral distortion continuing, though the rate of change has slowed. Figure 3.14 was taken at 2.0 meters, where the distortion has slowed down and the spectrum has not changed compared to the 1.6 meter data.

Figure 3.15 shows the previous far microphone data at positions of 0.4, 0.8, and 1.2 meters, labeled A, B, and C respectively. Typical spectra from subsonic jets diminish at a rate of $1/f^2$ whereas the slope of supersonic jet spectra have a slope of $1/f$. These rates of rolloff correspond to 20 dB per decade and 26 dB per decade, respectively. This data in Figure 3.15 show these trend, with the rate of decrease for spectrum A being approximately 21 dB per decade, for B, 23 dB per decade, and 27 dB per decade for spectrum C. Thus the spectral data

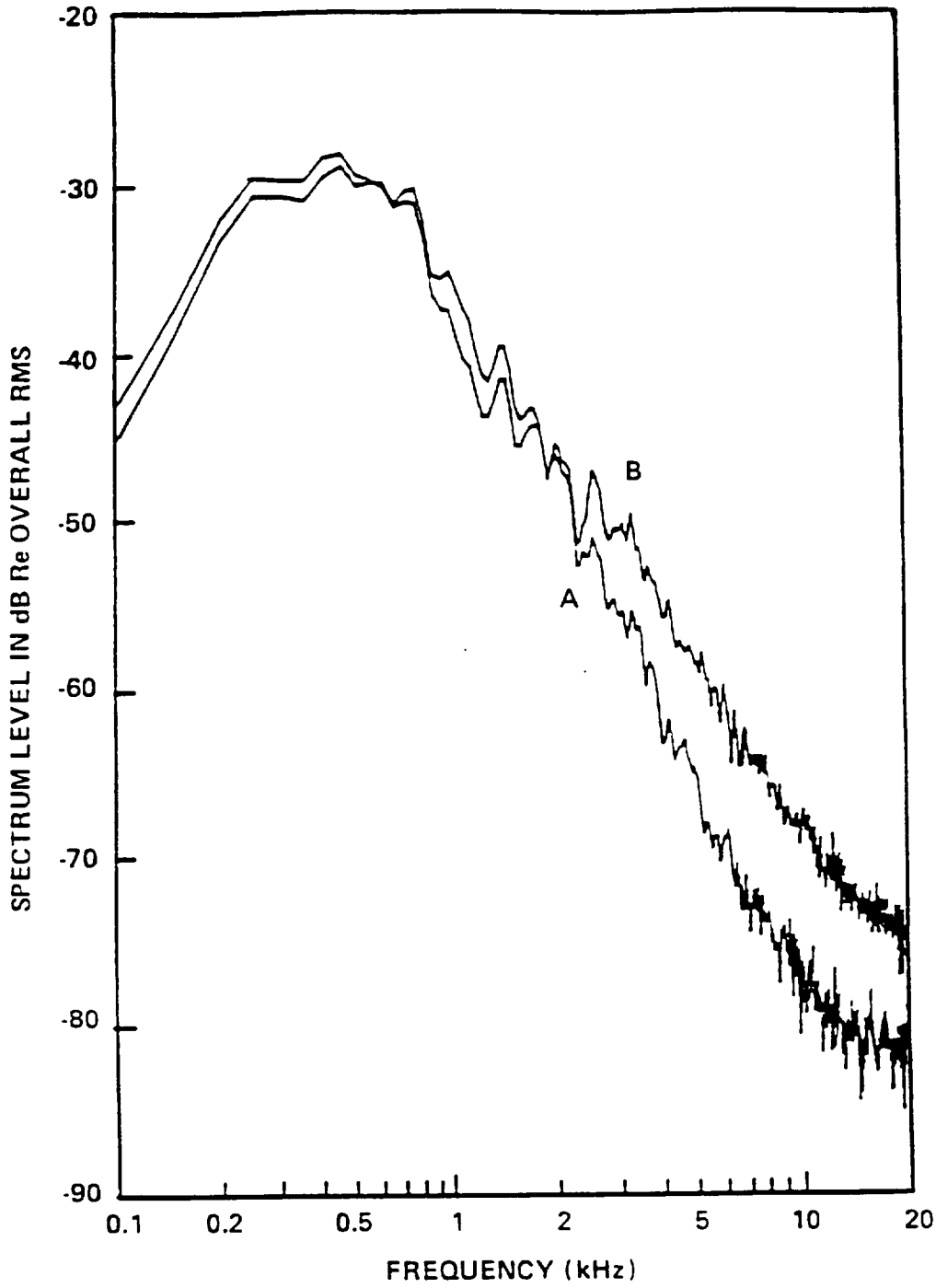

Figure 3.10 Spectral Data, High Level Distortion, 0.4 Meters from Source

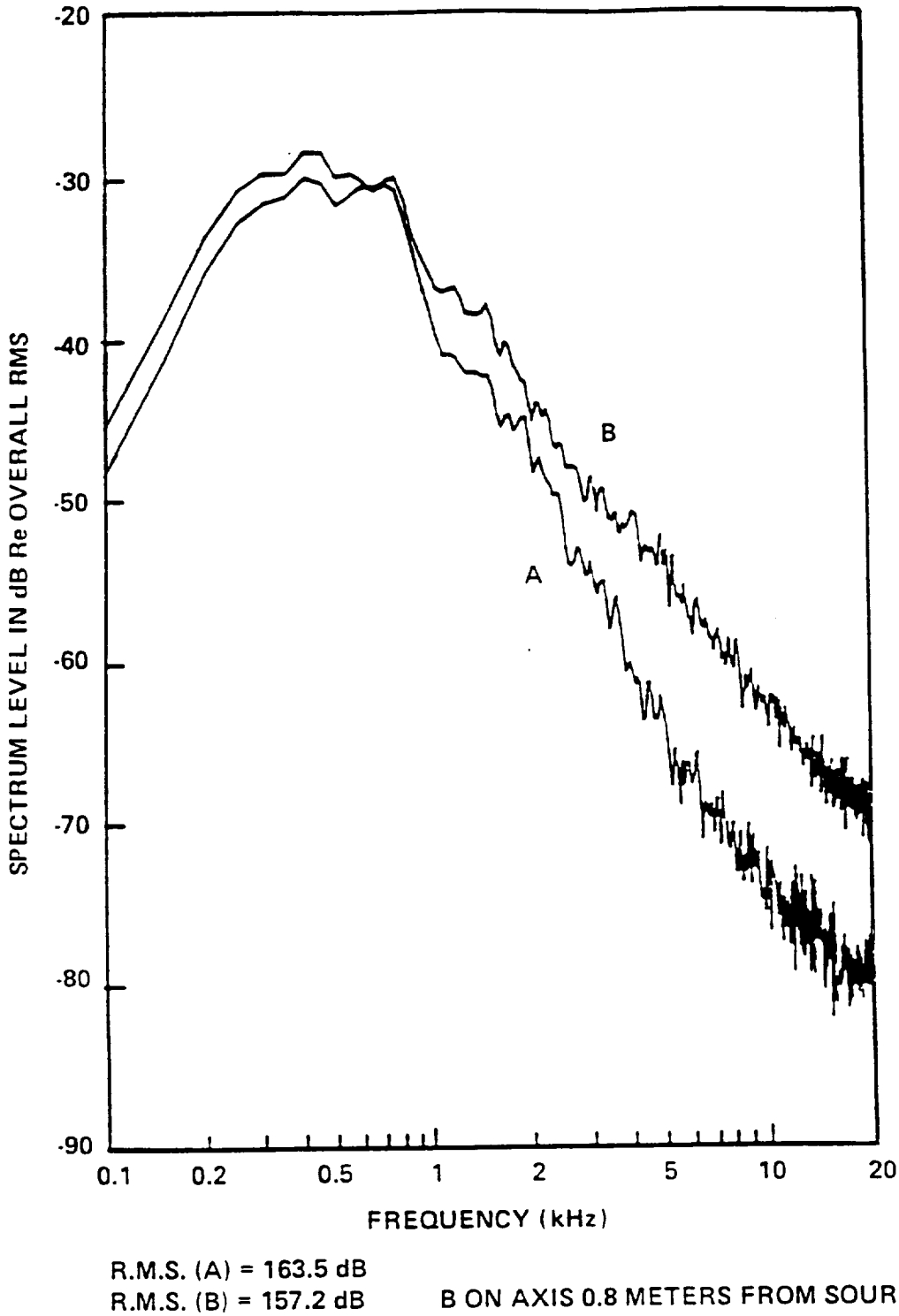

Figure 3.11 Spectral Data, High Level Distortion, 0.8 Meters from Source

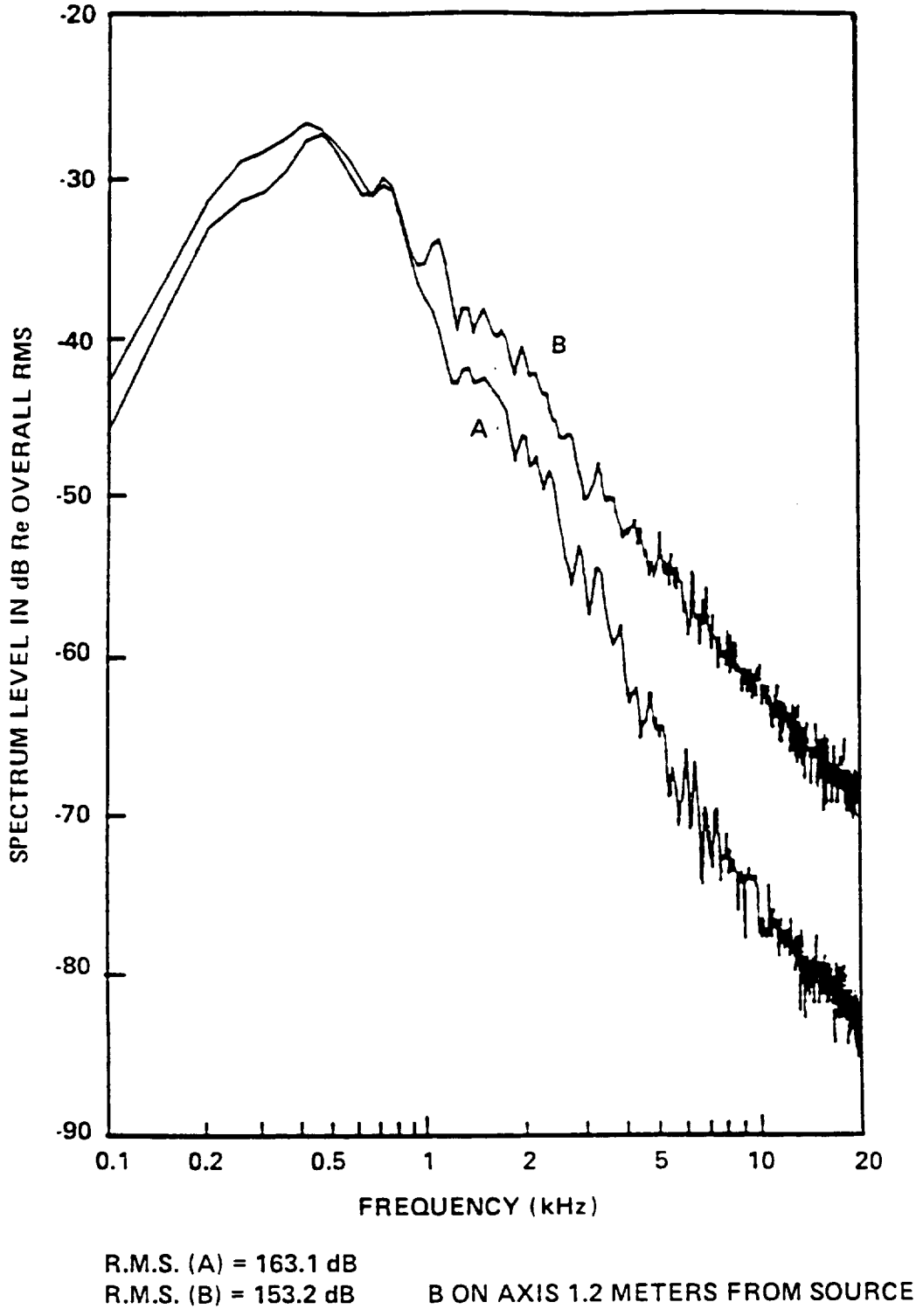

Figure 3.12 Spectral Data, High Level Distortion, 1.2 Meters from Source

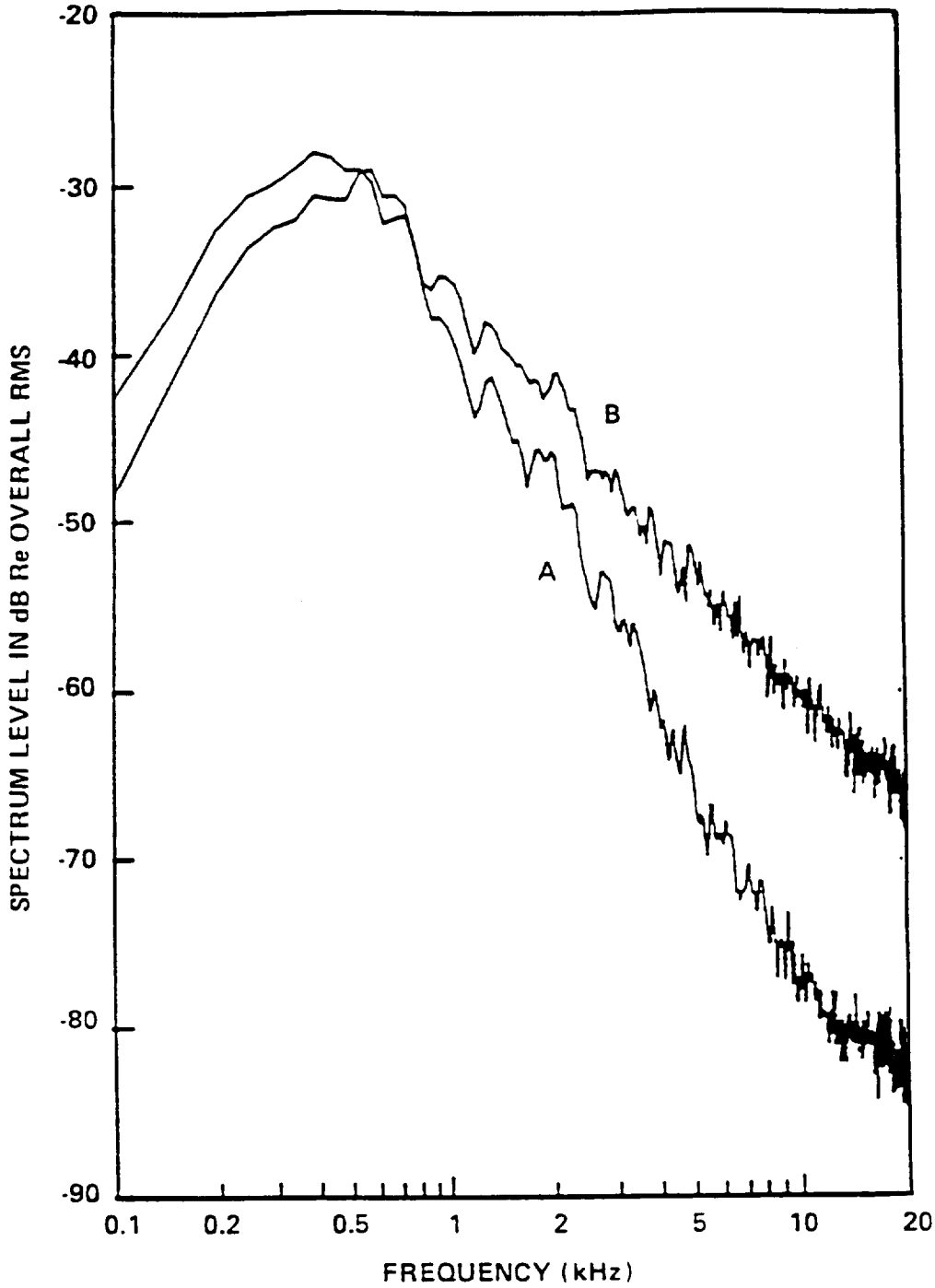

Figure 3.13 Spectral Data, High Level Distortion, 1.6 Meters from Source

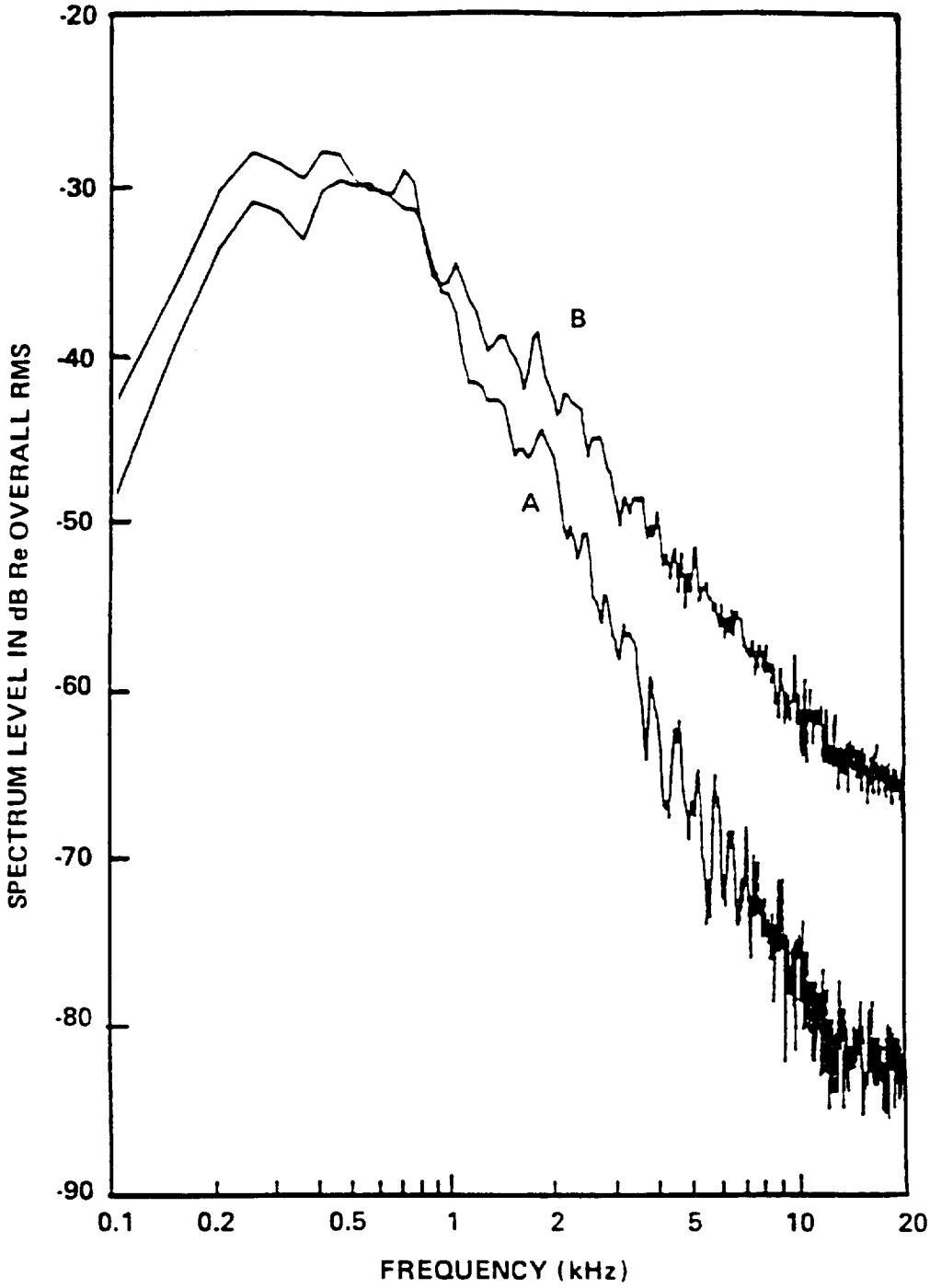

Figure 3.14 Spectral Data, High Level Distortion, 2.0 Meters from Source

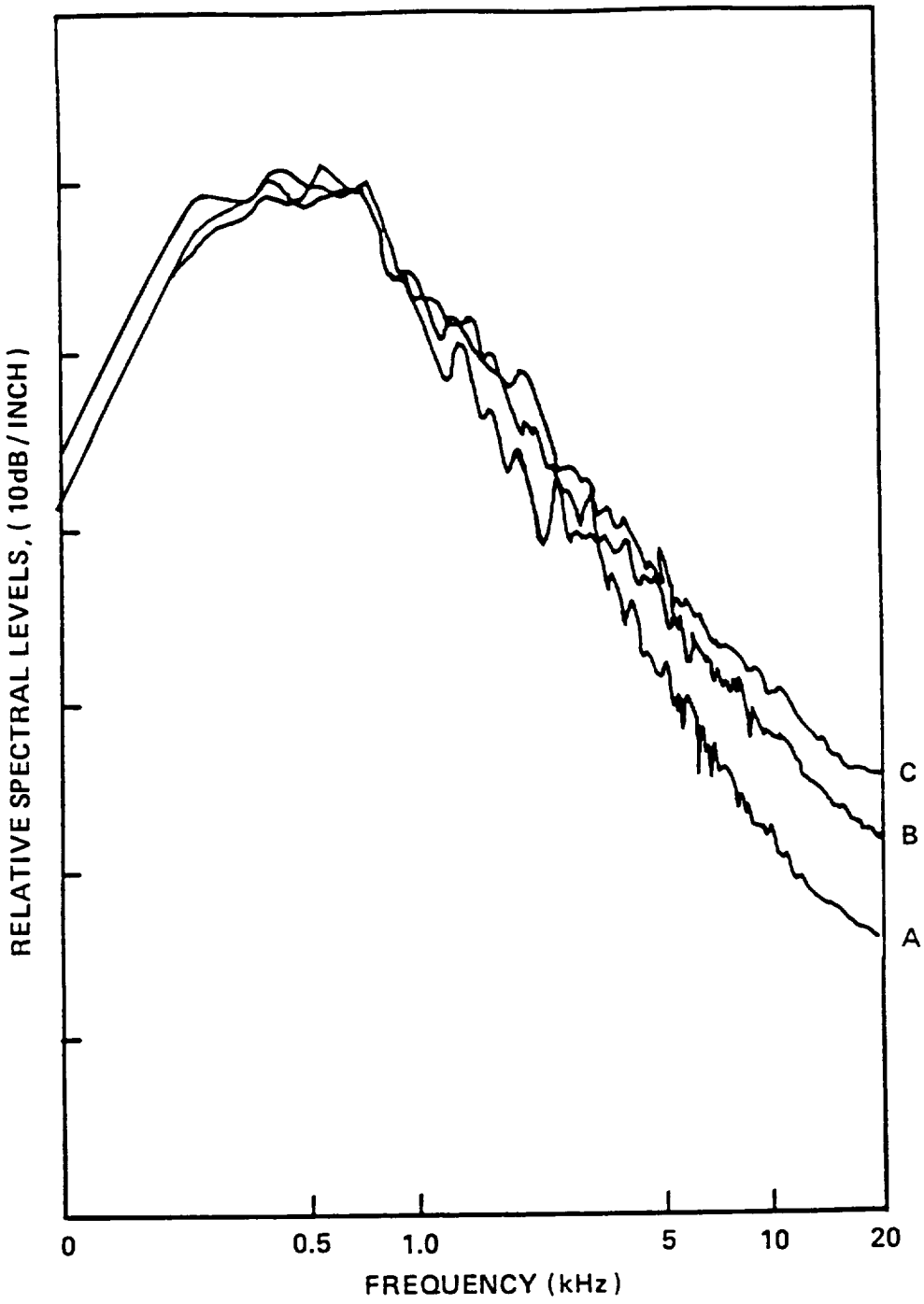

Figure 3.15 Comparison of Spectra at 0.4, 0.8, and 1.2 Meters

shows that as the high intensity signal propagates the spectral shape is quickly approaching the shape of data from supersonic jet aircraft.

CHAPTER 4

COMPARISON WITH AN EXISTING THEORETICAL MODEL

Introduction

A numerical model used to investigate the propagation of high amplitude acoustic signals was developed at PSU just prior to the onset of this research. This model was utilized with some modification to demonstrate that the wave distortion and spectrum shifts observed in the experiments are caused by acoustic phenomena. This chapter discusses the model developed by McKendree [13], its use, and results.

Introduction to the Acoustic Nonlinear Model

McKendree's model uses a finite difference interpolation technique to obtain a lossless plane wave solution of Burger's equation as developed by Bellman [14]. An advantage of this technique is stability around shock regions and beyond. This technique also has no tendency to predict double valued solutions. These advantages make the model ideal for this research as the high frequency components of the noise signal reach their critical ranges in very short distances.

The model propagates a signal by interpolating values from the original signal time history that represent the signal at another time. The steps in time must be small. The velocity of propagation is proportional to the sound pressure amplitude, as dictated by the solution to Burger's equation.

The lossless Burger's equation can be written as shown by Khoklov [15]

$$\frac{\partial p}{\partial \sigma} - p\frac{\partial p}{\partial \tau} = 0 \quad . \tag{4-1}$$

For small steps in the propagation distance the derivative $\partial p/\partial \sigma$ is approximated by

$$\frac{1}{\sigma}[p(\sigma,\tau) - p(0,\tau)] \quad . \tag{4-2}$$

Using equations 4-1 and 4-2 and a Taylor's series expansion for $p(\sigma,\tau)$ for steps small enough that $\sigma(\partial p/\partial\tau)$ is small (i.e. $<< 1$) the solution can be written as

$$p(\sigma,\tau) = p[(0,\tau) + \sigma p(0,\tau)] \quad . \qquad (4-3)$$

The equation solving algorithm begins with a waveform described by values of $p(\sigma,0)$ through $p(\sigma,\tau)$. From these values the values at $p(\sigma+\Delta\sigma,\tau+\Delta\tau)$ are computed. These values are used in the next small step in σ. Equation 4-3 is used again and again to propagate the signal to the desired range. The model uses a linear interpolator because of its stability around shock regions that other techniques did not exhibit. This method can however underestimate the values around the shock region thus lessening the severity of the shock region. This is shown in the comparisons to measured data that follow. The accuracy of the solution can be improved by using smaller steps in time, at the expense of computer time.

Modifications Made to the Model

The noise signals presented in the previous chapter are spherically diverging at the higher frequencies. The model developed by McKendree using the equations above was developed and tested for plane wave propagation. In order to use the model to propagate signals comparable to those measured, the program developed by McKendree was modified. The modifications are presented below.

Using a transformation developed by Naugol'nykh et. al [16] equation (4-3) can be applied to spherical wave propagation. The transformation redefines σ and τ as shown in equations 4-4 and 4-5.

$$\sigma = \beta\epsilon k r_o \ln(r/r_0) \qquad (4-4)$$

$$\tau = \omega(t - r/r_0) \qquad (4-5)$$

These definitions were entered in the model to make the predictions presented in this chapter.

Application of the Model to Sine Wave Data

The model's validity was tested by propagating a pure tone signal. From such a test the model's predictions can be compared to classical solutions. One parameter of interest is the shock formation distance, where the shock wavefront becomes infinitely steep. The shock formation distance, r_c can be calculated using

$$r_c = r_0 e^{(1/\sigma_0)} \qquad (4-6)$$

for spherical waves, where r_0 is the "Rayleigh distance" for a projector of area A_0, $\sigma_0 = \beta_0 \epsilon_0 k_0 r_0$ is the scaled range parameter. Figure 4.1 shows shock formation distances as a function of peak level for a pure tone at 1000 Hz. At 170 dB peak level, the shock distance is approximately 0.8 meters.

Shown in Figure 4.2 is the 1000 Hz sine wave input to the model and the waveform after being propagated 0.2 meters. In this figure the distortion is just beginning. The data are normalized as in Chapter 3 by dividing each waveform by the maximum pressure in the waveform to account for the differences in the amplitudes. In Figure 4.3 the waveform has propagated 0.4 meters and the distortion process has greatly steepened the wavefronts. Figure 4.4 shows just two cycles of the data to better illustrate the steepness of the waveform. In Figure 4.5, at 0.6 meters, the waveform has almost reached the complete shock shape. At 0.8 meters, shown in Figure 4.6, the waveform has reached the classical "inverted N" shape that is indicative of an acoustic pressure waveform that has reached its shock formation distance. Figure 4.7 shows just two cycles of the data to more clearly show the waveform shape. Shown in Figure 4.8 is the waveform

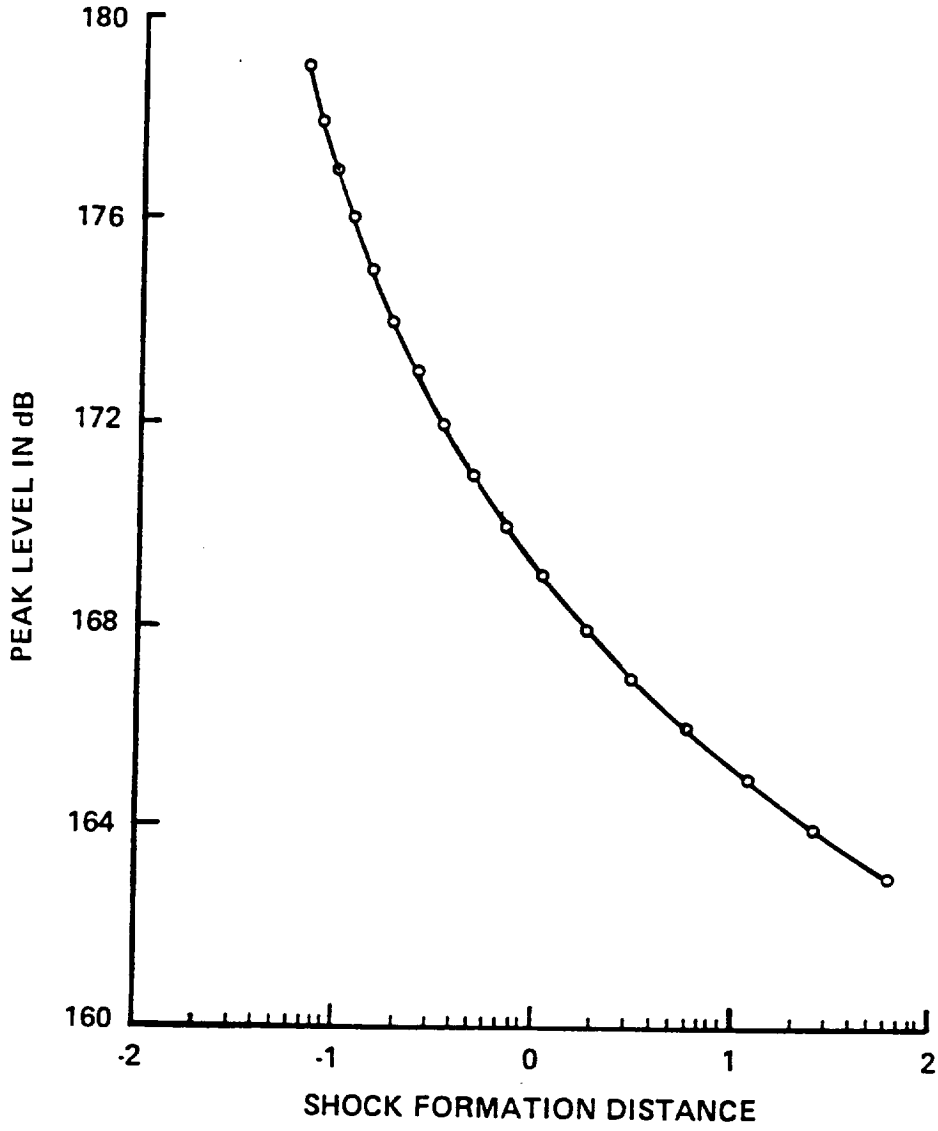

Figure 4.1 Shock Formation Distance vs. Level at 1000 Hz.

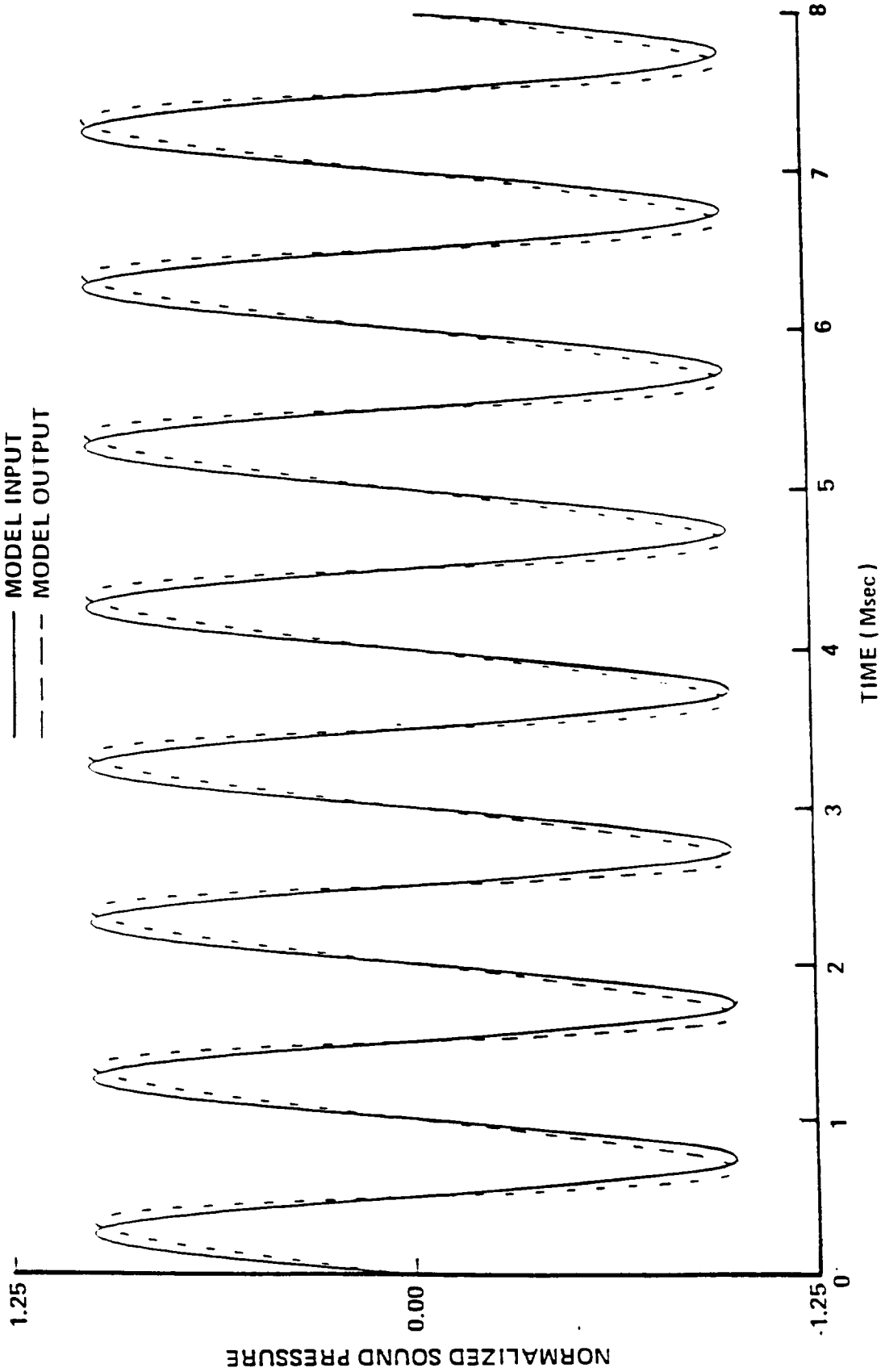

Figure 4.2 Input 1000 Hz., 170 dB Peak Wave, Propagated Wave at 0.2 Meters

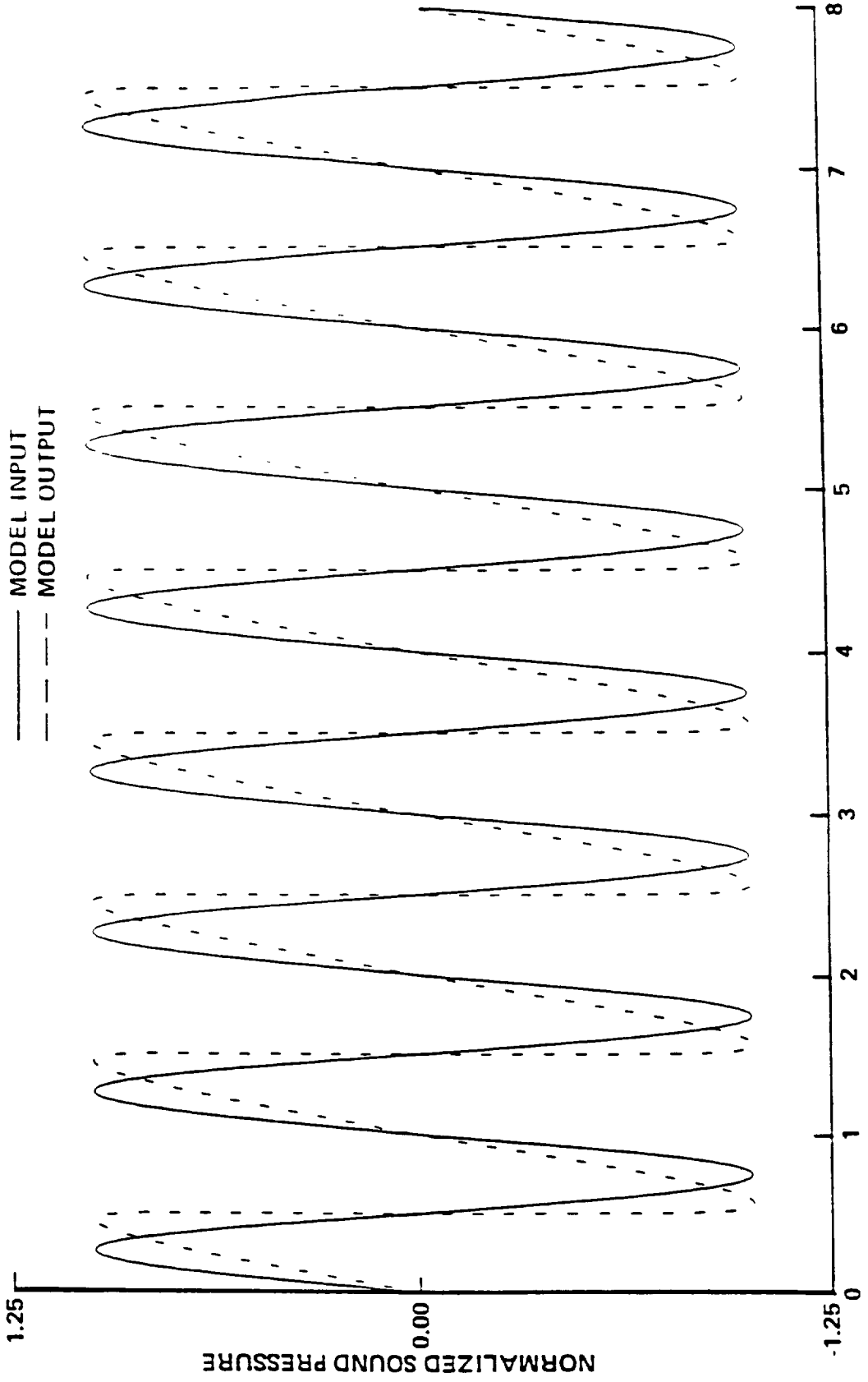

Figure 4.3 Input 1000 Hz., 170 dB Peak Wave, Propagated Wave at 0.4 Meters

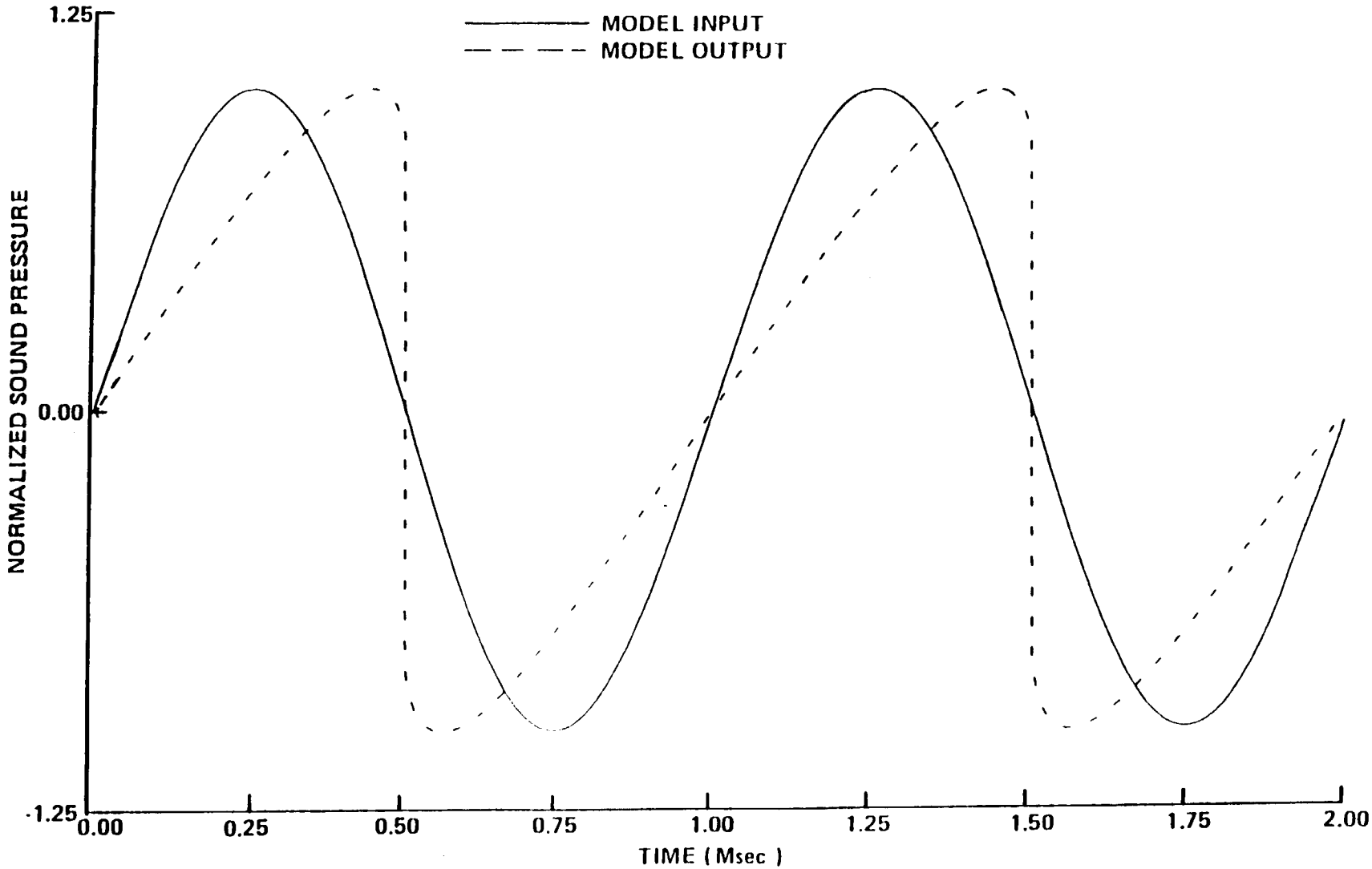

Figure 4.4 Two Cycles of Input and Propagated Waveform at 0.4 Meters

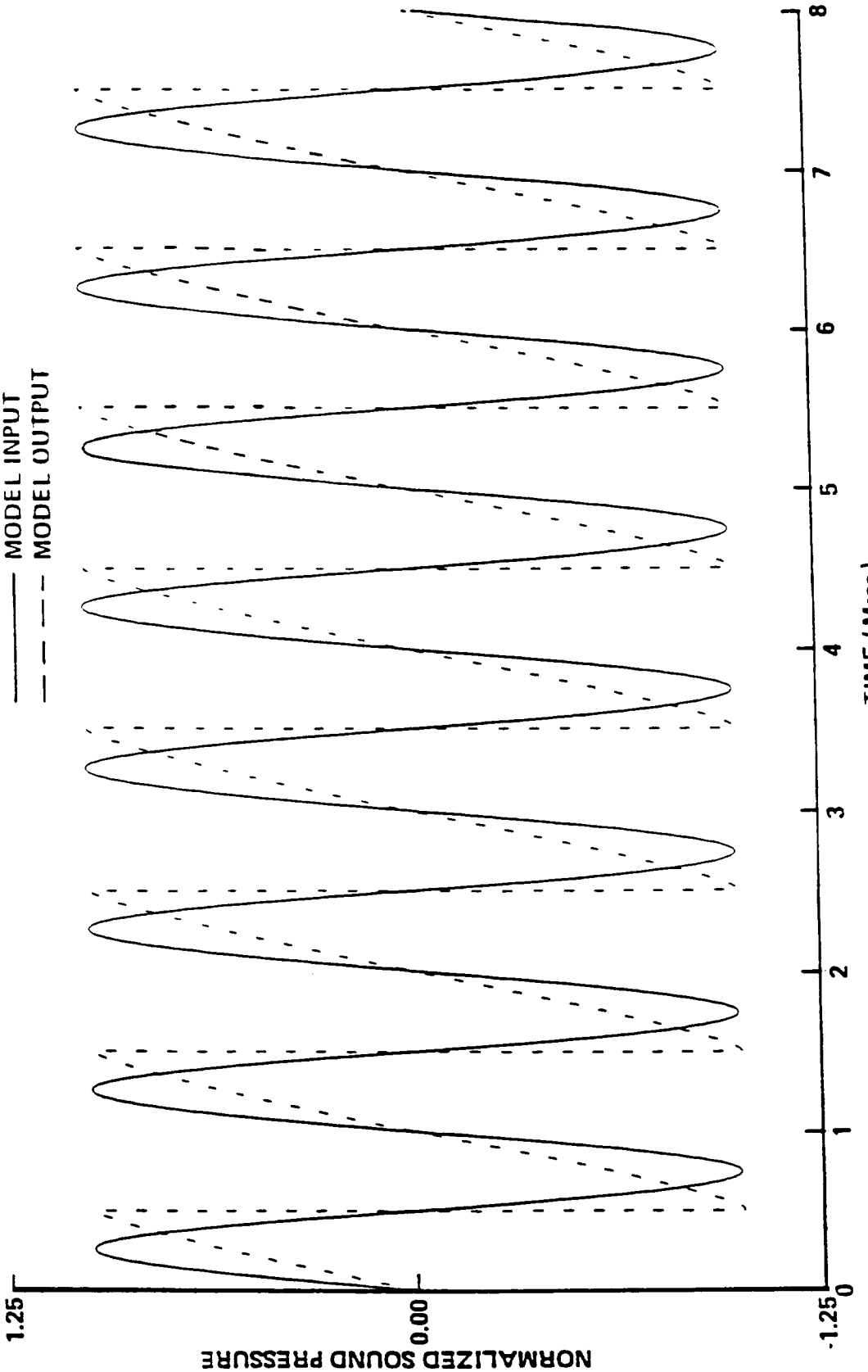

Figure 4.5 Input 1000 Hz., 170 dB Peak Wave, Propagated Wave at 0.6 Meters

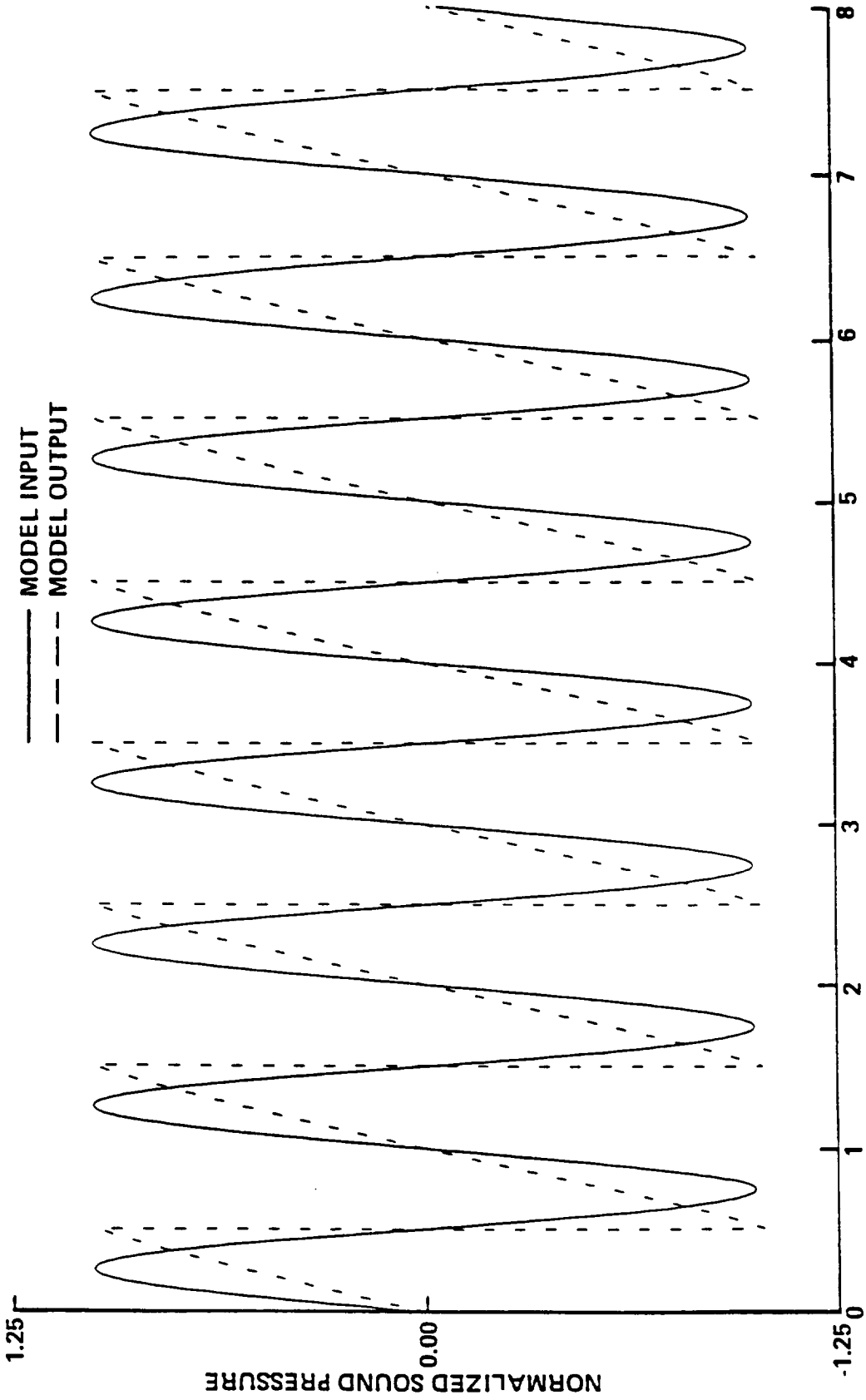

Figure 4.6 Input 1000 Hz., 170 dB Peak Wave, Propagated Wave at 0.8 Meters

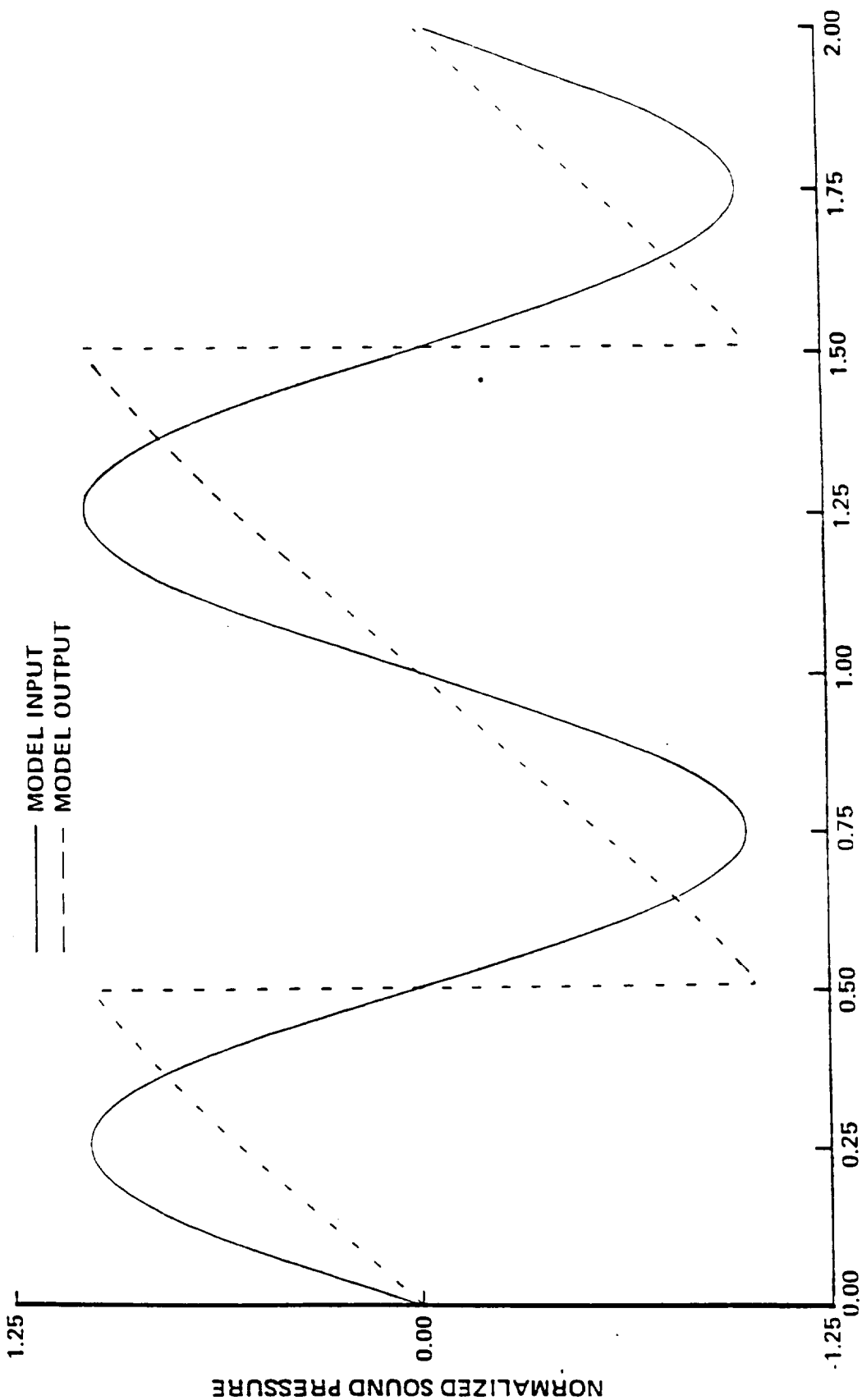

Figure 4.7 Two Cycles of Input and Propagated Waveform at 0.8 Meters

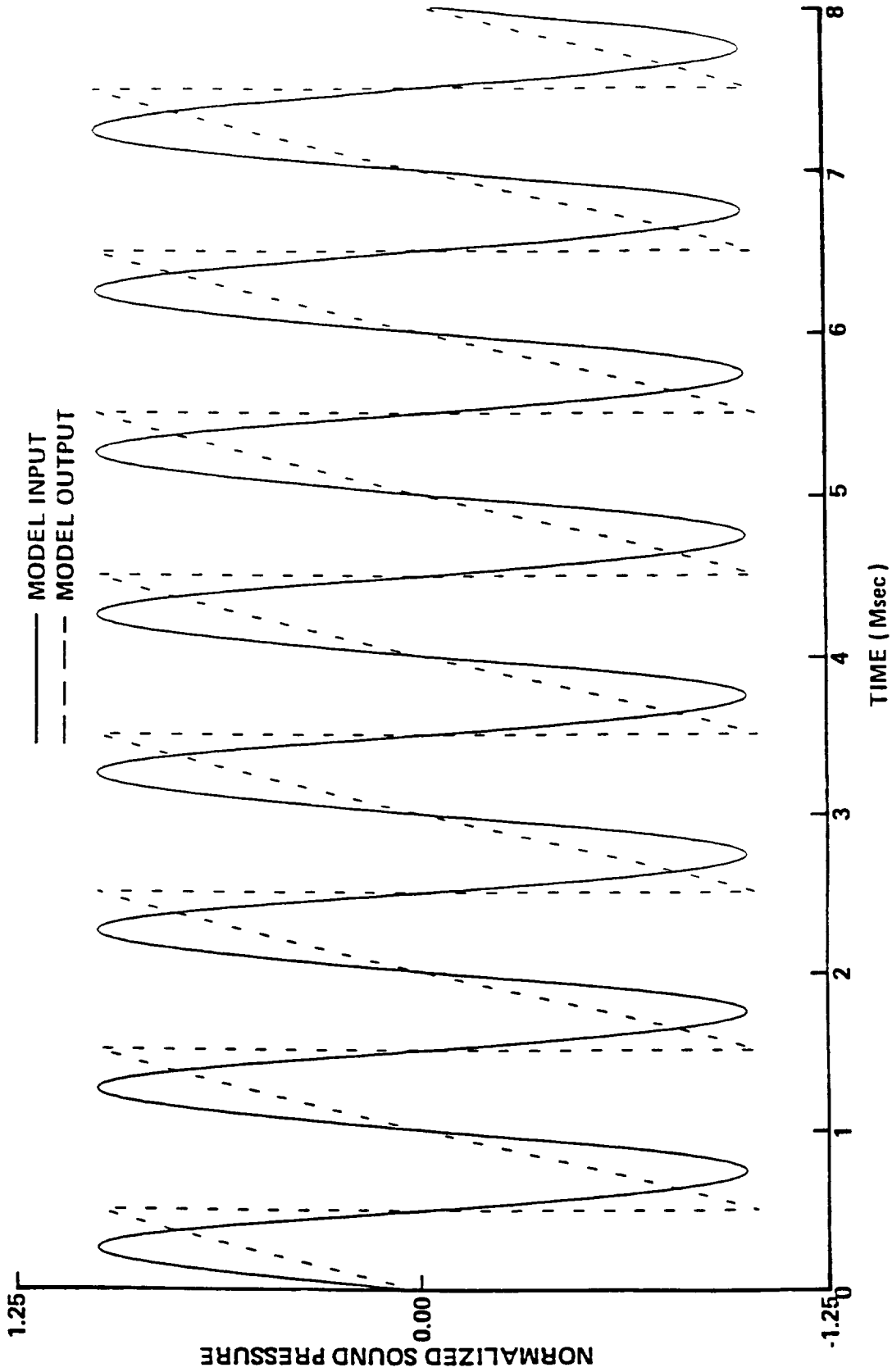

Figure 4.8 Input 1000 Hz., 170 dB Peak Wave, Propagated Wave at 1.0 Meters

at 1.0 meters, beyond the shock formation distance. The shape of the wave has not changed, and the model has not predicted a double valued pressure signal.

These data show that the model does predict the waveform shape up to, and beyond, the critical range. More importantly, the model accurately predicts the rate at which the shock forms. These results are important for the model to accurately predict noise waveform propagation which consist of abundant frequencies. These results are presented next.

Application of the Model to Noise Data

The input data were generated using a digital random signal generator with band limited frequencies. These signals were then amplified to represent the acoustic pressures measured in the experiment. The noise waveforms were then propagated over ranges of 0.4 to 2.0 meters. The data output by the model were propagated signal time histories at specified distances throughout the total propagation distance. Some results are presented in this section.

Figures 4.9 through 4.14 show a "low level" waveform as it propagates. The data were output every 0.4 meters of propagation distance, thus Figure 4.9 is at 0.4 meters, Figure 4.10 is at 0.8 meters, etc. The maximum amplitude of these data is 355 N/M^2 (145 dB). In Figure 4.9 the two waveforms are indistinguishable as the distortion has not had an effect. At 0.8 meters, Figure 4.10, the waveform is beginning to lead and lag at the extreme pressures for the higher amplitude components. At 1.2 meters the distortion is becoming more apparent, as was seen in the measured data. Figure 3-1, which shows data measured at 1.2 meters from the source, shows similar characteristics to the data in Figure 4.11, with the propagated waveform showing slight leads and lags at the extremes pressures, and little or none for the lower pressures. Figure 4.12 shows the data at 1.6 meters, and can be compared to Figure 3-2. Here the data are showing distortion

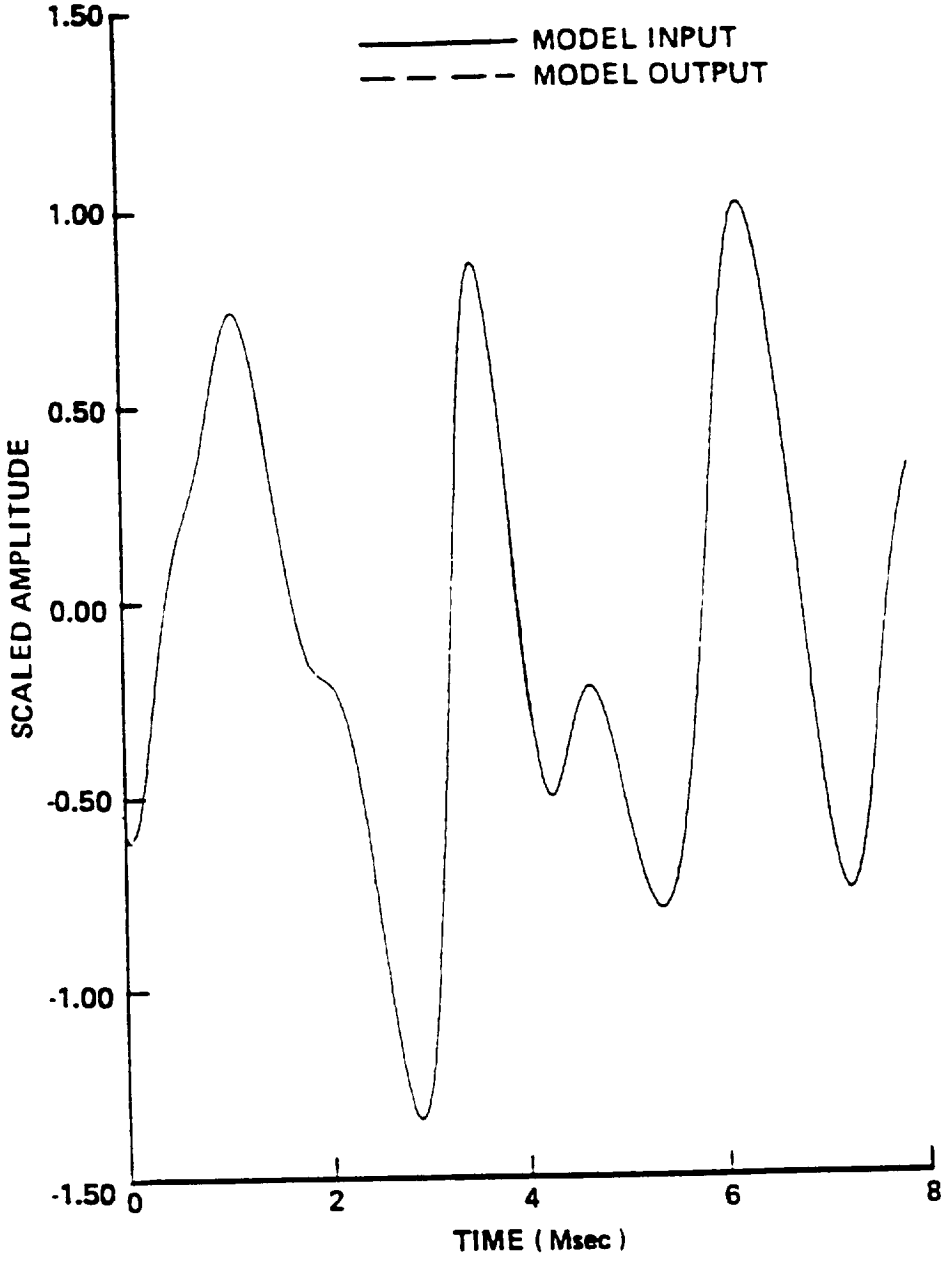

Figure 4.9 Model Output at 0.4 Meters for a 145 dB Random Noise Waveform

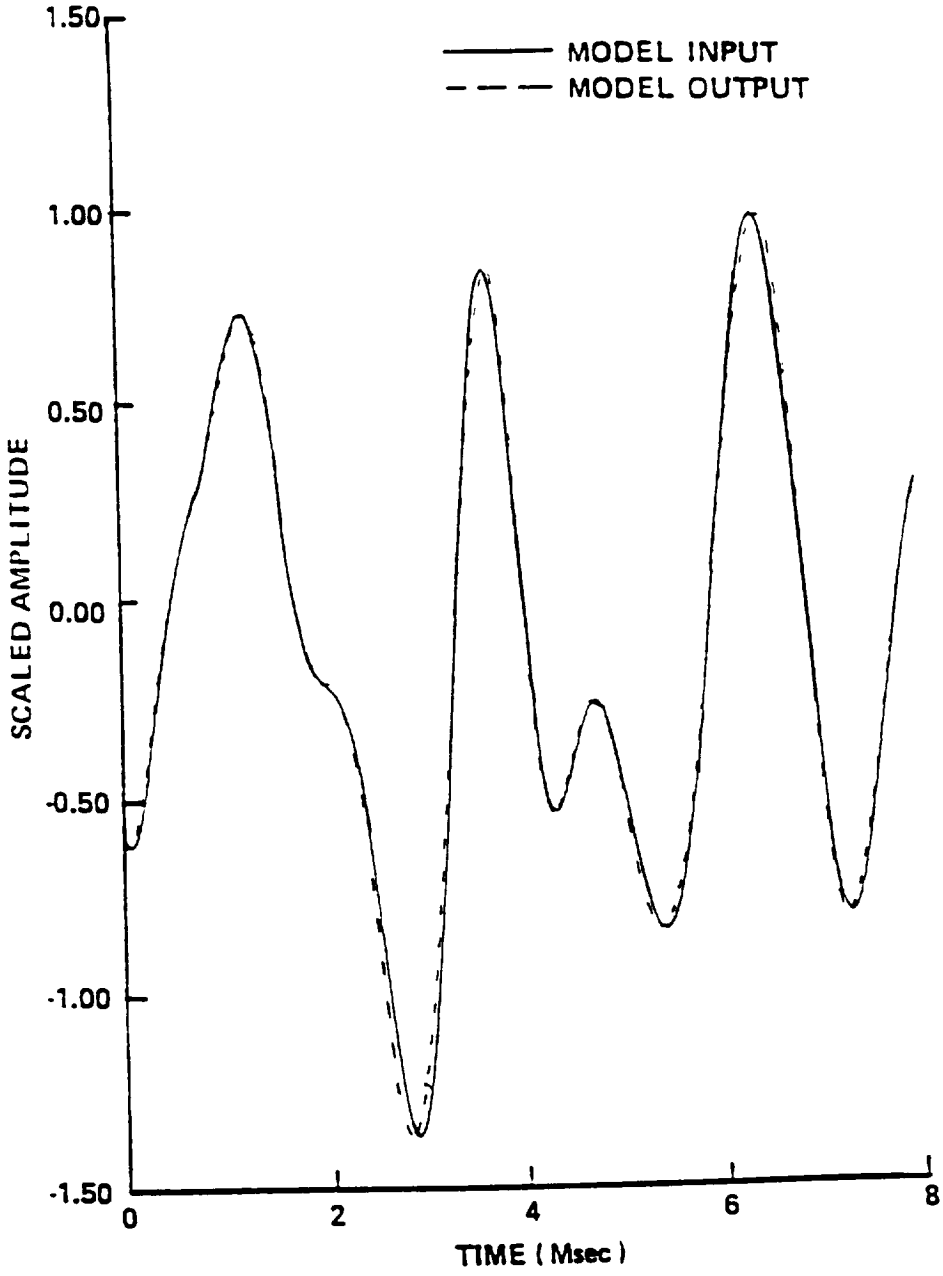

Figure 4.10 Model Output at 0.8 Meters for a 145 dB Random Noise Waveform

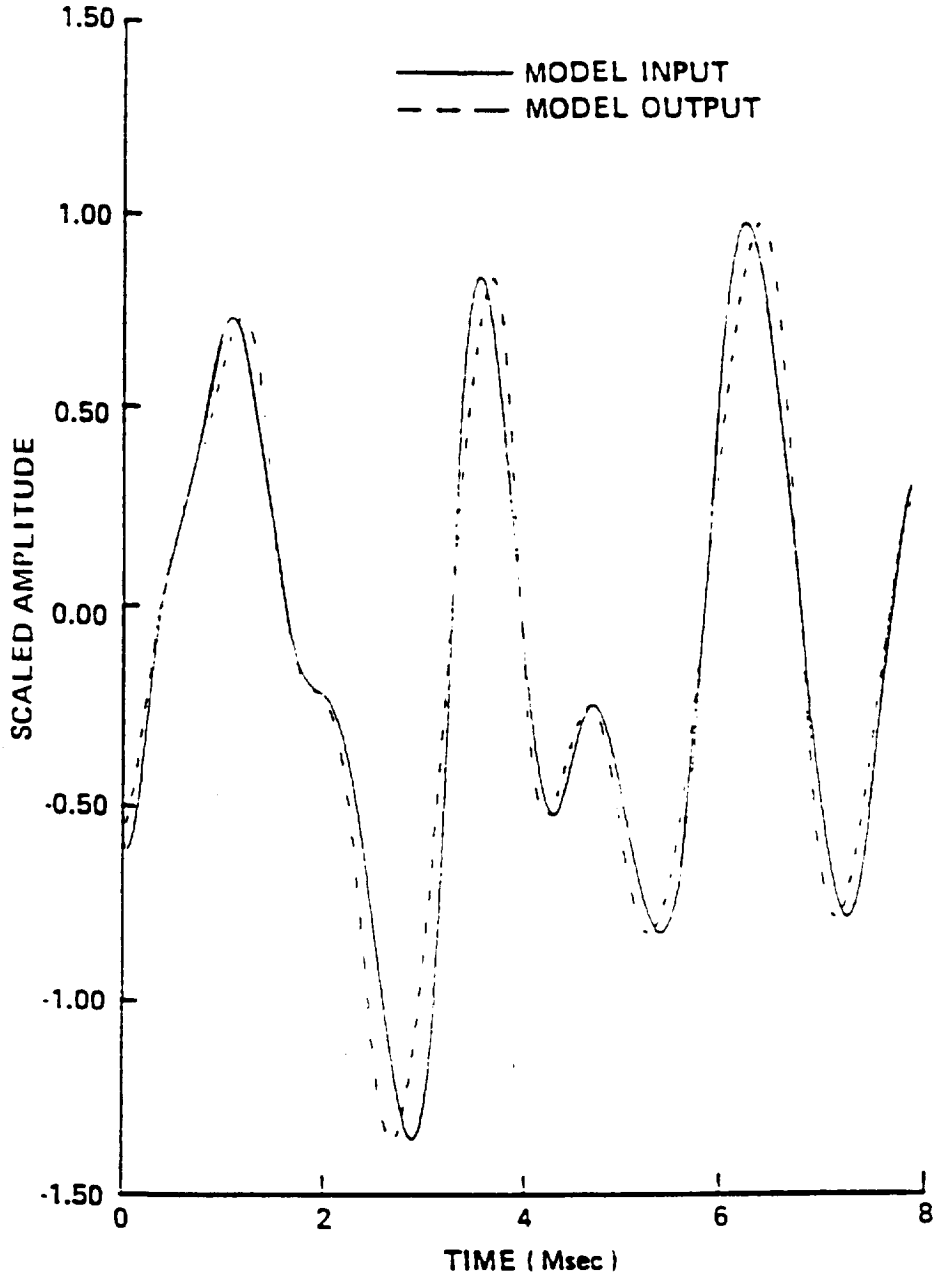

Figure 4.11 Model Output at 1.2 Meters for a 145 dB Random Noise Waveform

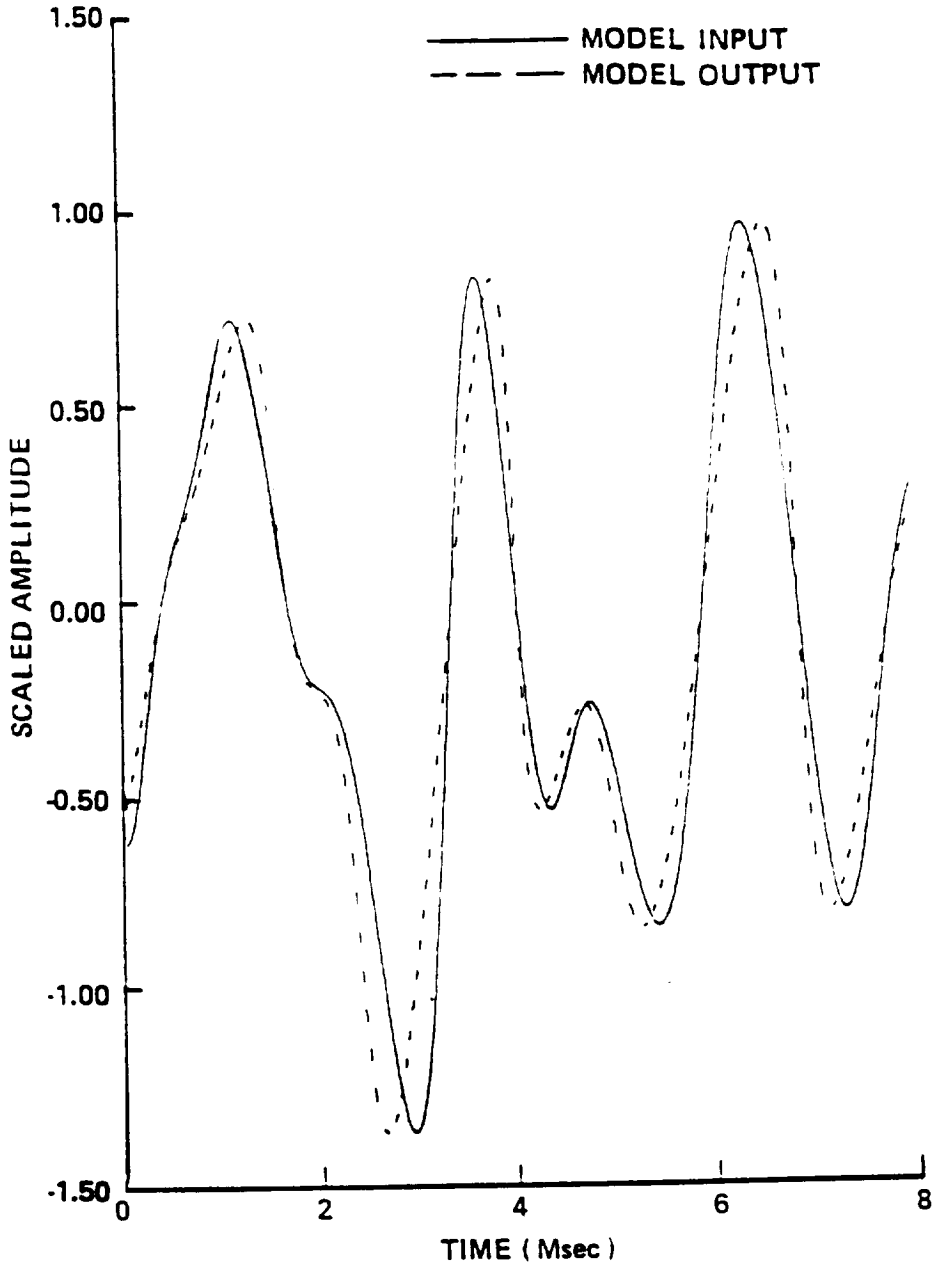

Figure 4.12 Model Output at 1.6 Meters for a 145 dB Random Noise Waveform

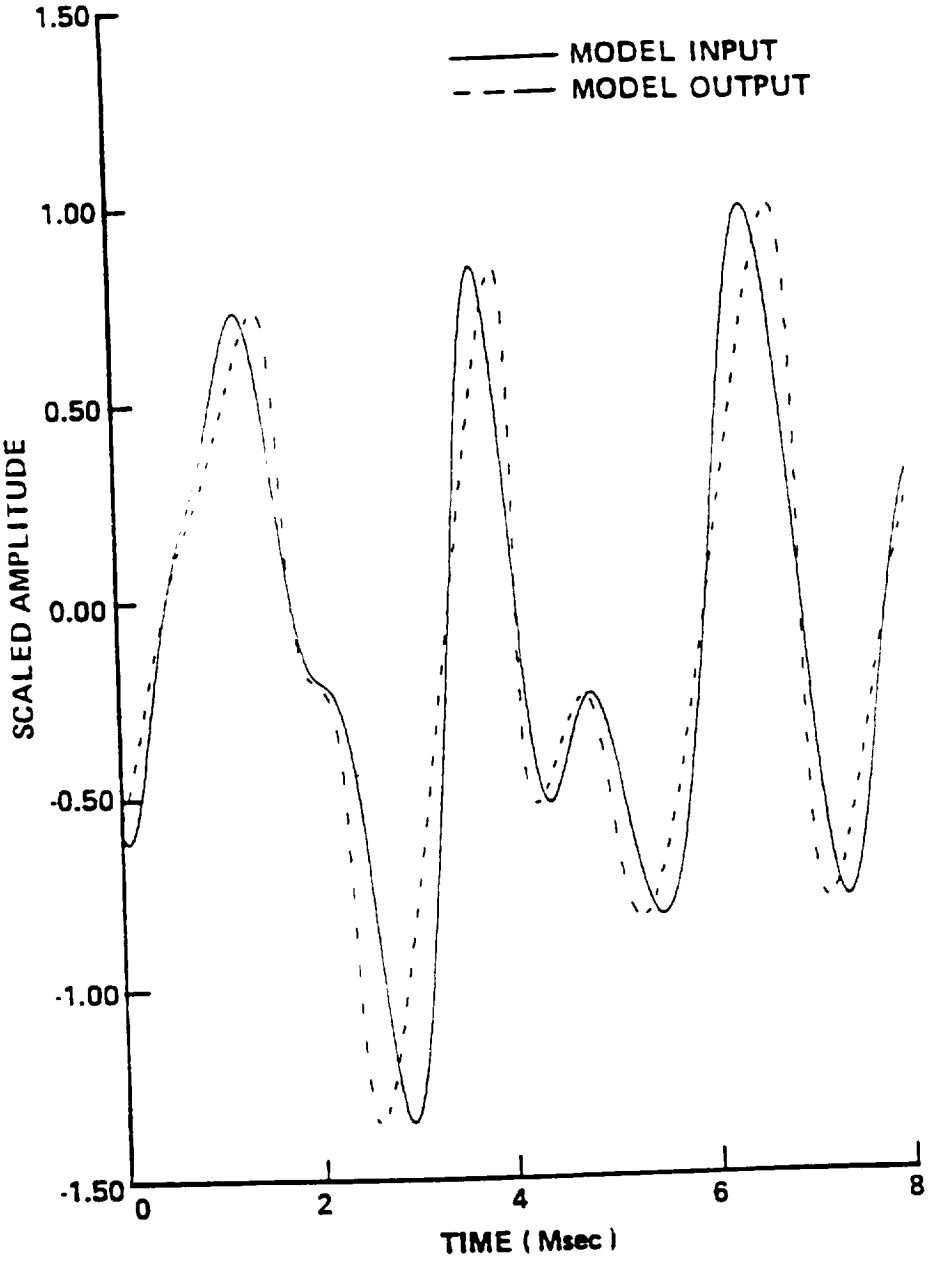

Figure 4.13 Model Output at 2.0 Meters for a 145 dB Random Noise Waveform

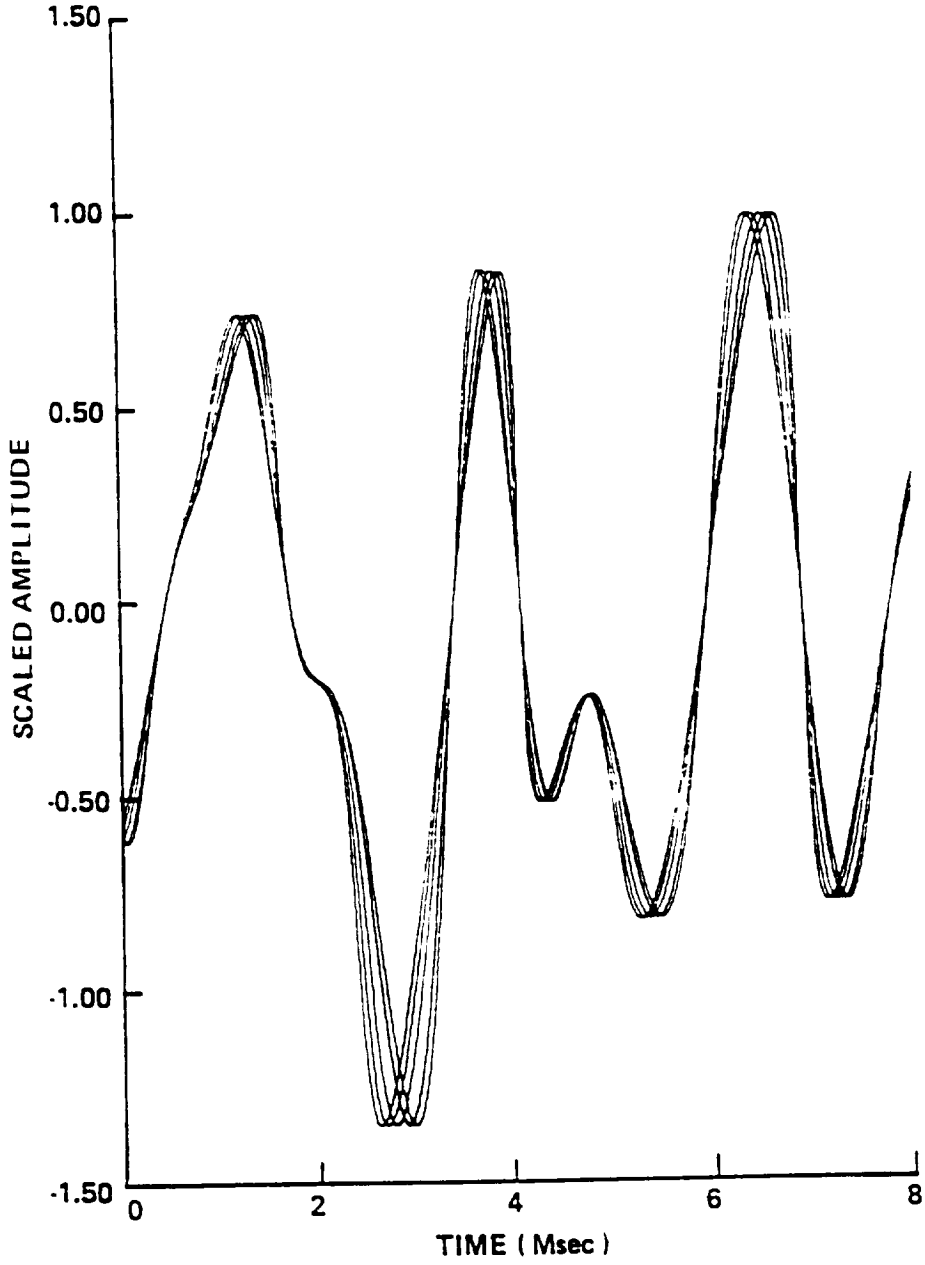

Figure 4.14 Overlay of Model Output for 145 dB Random Noise Waveforms

effects for the entire waveform. Finally, Figure 4.13 shows the distortion at 2.0 meters. Again, the waveform is becoming more distorted, and the shock fronts are becoming very steep. The fact that the model is based on a lossless form of Burger's equation has the effect of making the shocks steeper than those measured. This will become more apparent later. Figure 4.14 shows all the waveforms, and illustrates the effects of amplitude on the waveform distortion.

Figures 4.15 through 4.19 show the model output for a waveform having a maximum pressure of 1125 N/M^2 (155 dB). As before, the outputs are at every four tenths of a meter. The waveform 0.4 meters from the source, Figure 4.15, shows no distortion, as before. However, at this higher amplitude the distortion becomes apparent by the 0.8 meter location as seen in figure 4.16. Comparing these data to the data presented in Figure 3.4 shows that the model is predicting the waveform steepening rather well. By the time the waveform has arrived at the 1.2 meter location, shocks have already formed for the high frequency components of the waveform (Figure 4.17). As mentioned previously, the shock thickness is much less than observed in the measurements (Figure 3-5) due to the lossless assumption made in the development of the model. As the waveform propagates, this lossless assumption causes the distortion to be much greater than that measured. Figure 4.18 shows the model output at 1.6 meters, and Figure 4.19 at 2.0 meters. The model output does show a trend observed in the measured data which hasn't been accounted for. Referring back to Figure 3-6, which shows data of 156 dB maximum at 2.2 meters, one observes that around 0.004 seconds the trough of the distorted waveform has a lower pressure ratio that is caused by the distortion. This phenomenon is also predicted by the model, as can be seen in Figure 4.19 just beyond the 0.002 second point.

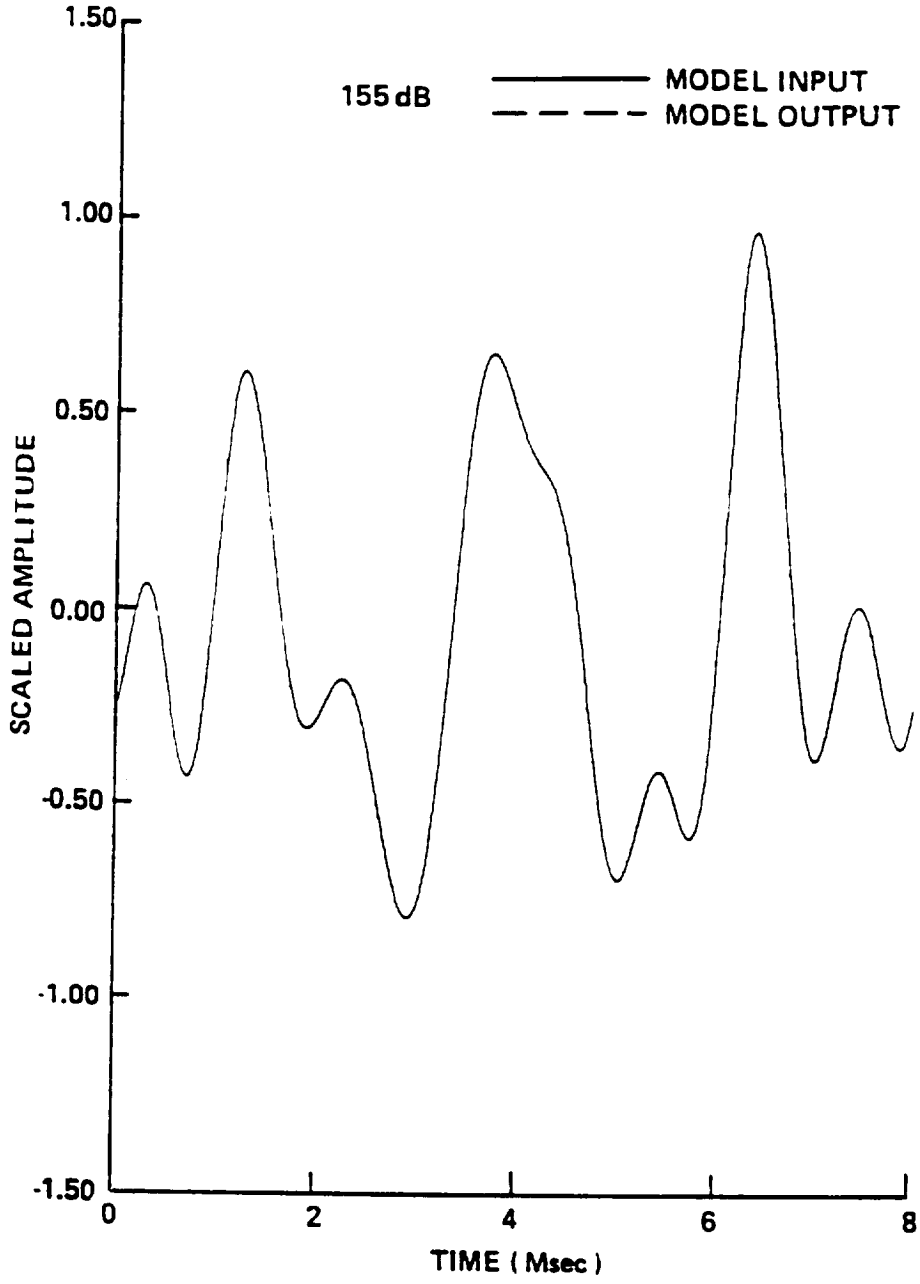

Figure 4.15 Model Output at 0.4 Meters for a 155 dB Random Noise Waveform

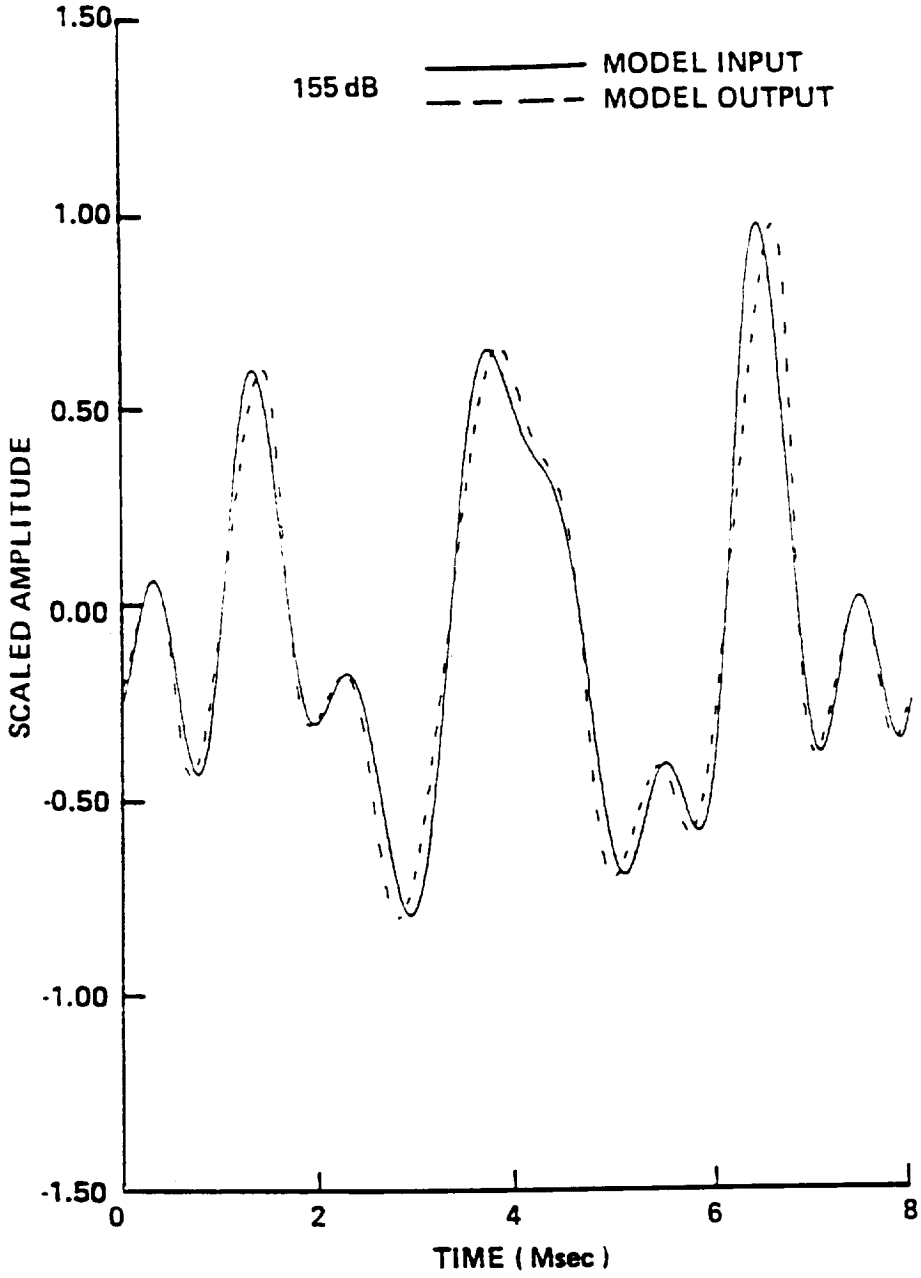

Figure 4.16 Model Output at 0.8 Meters for a 155 dB Random Noise Waveform

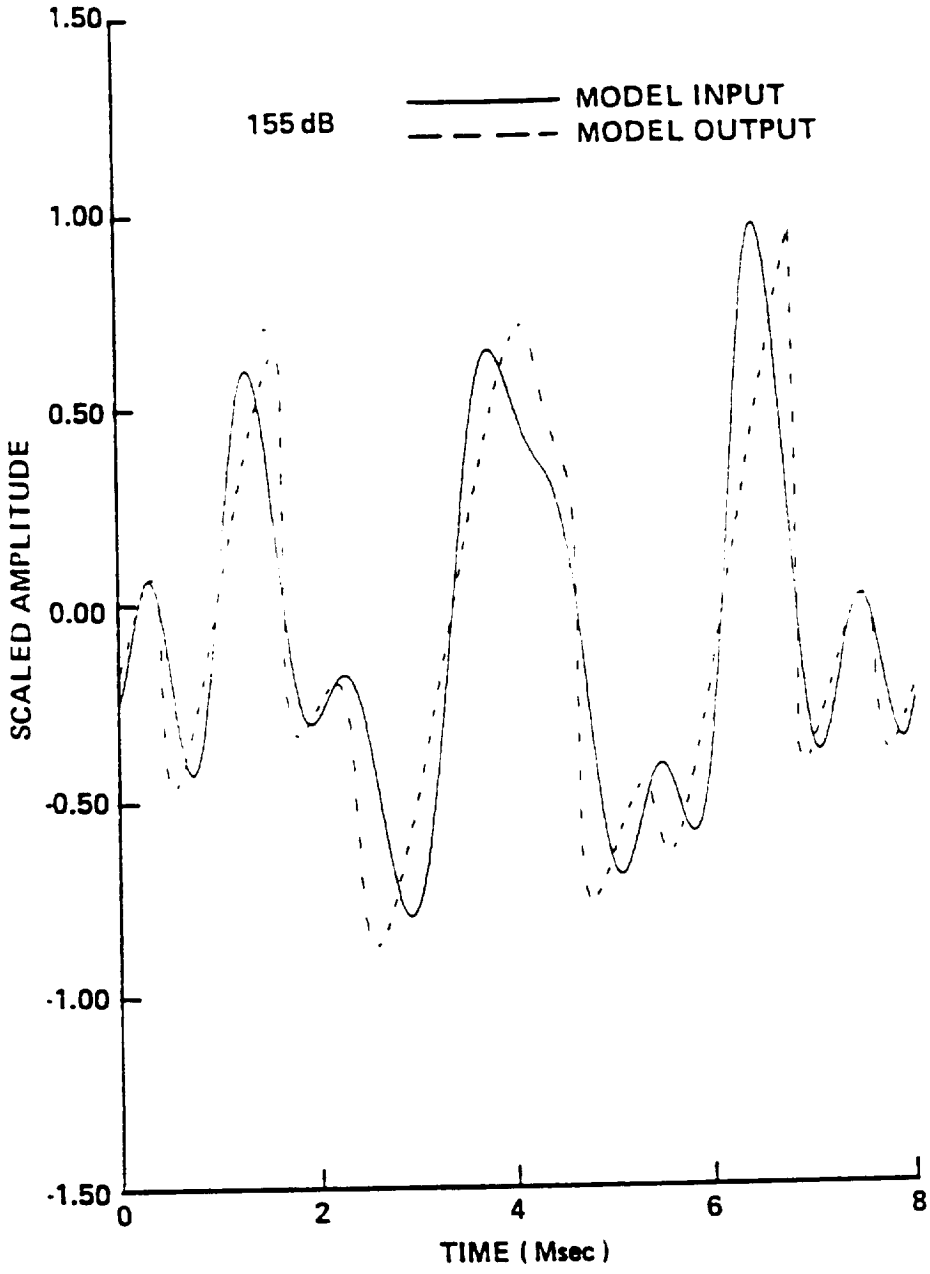

Figure 4.17 Model Output at 1.2 Meters for a 155 dB Random Noise Waveform

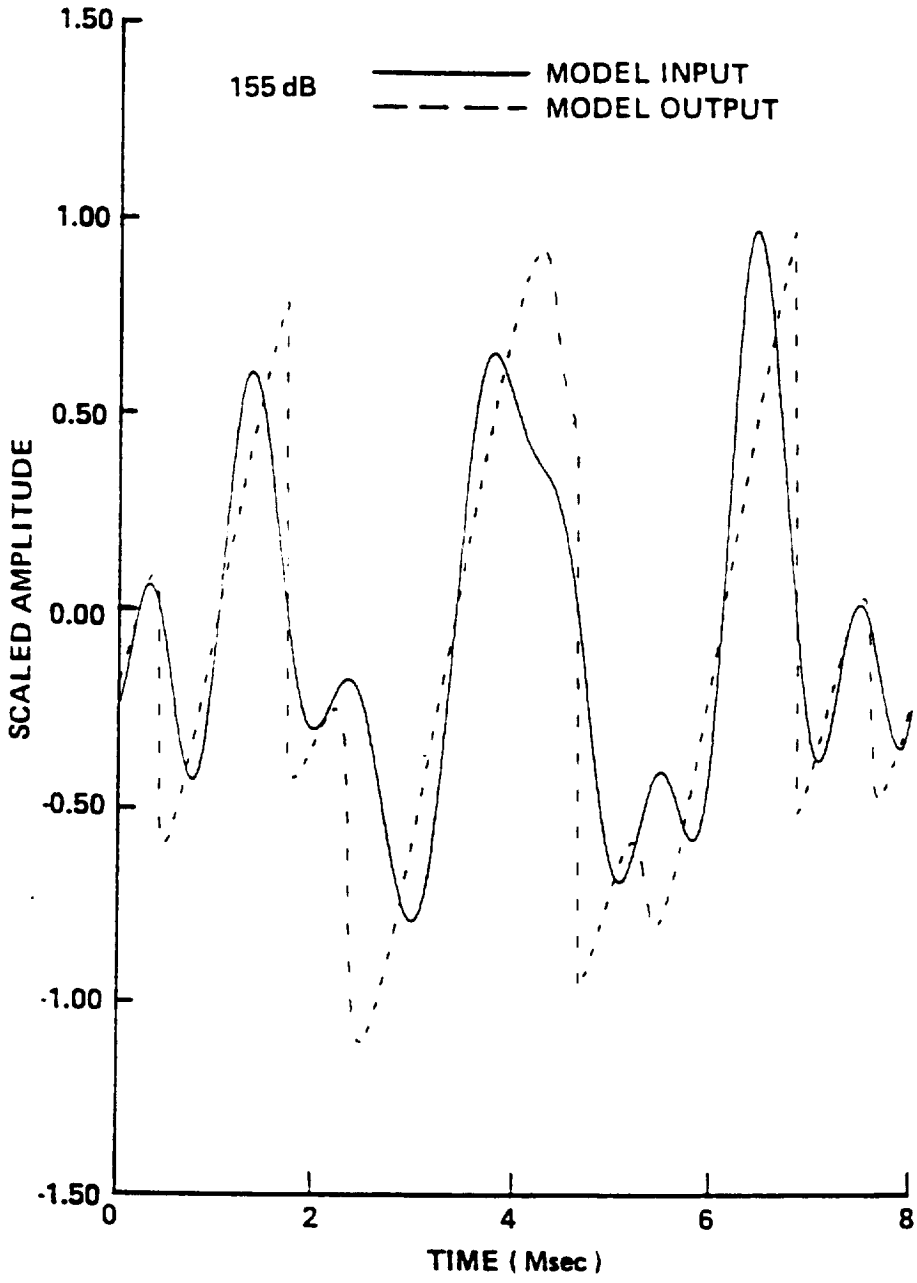

Figure 4.18 Model Output at 1.6 Meters for a 155 dB Random Noise Waveform

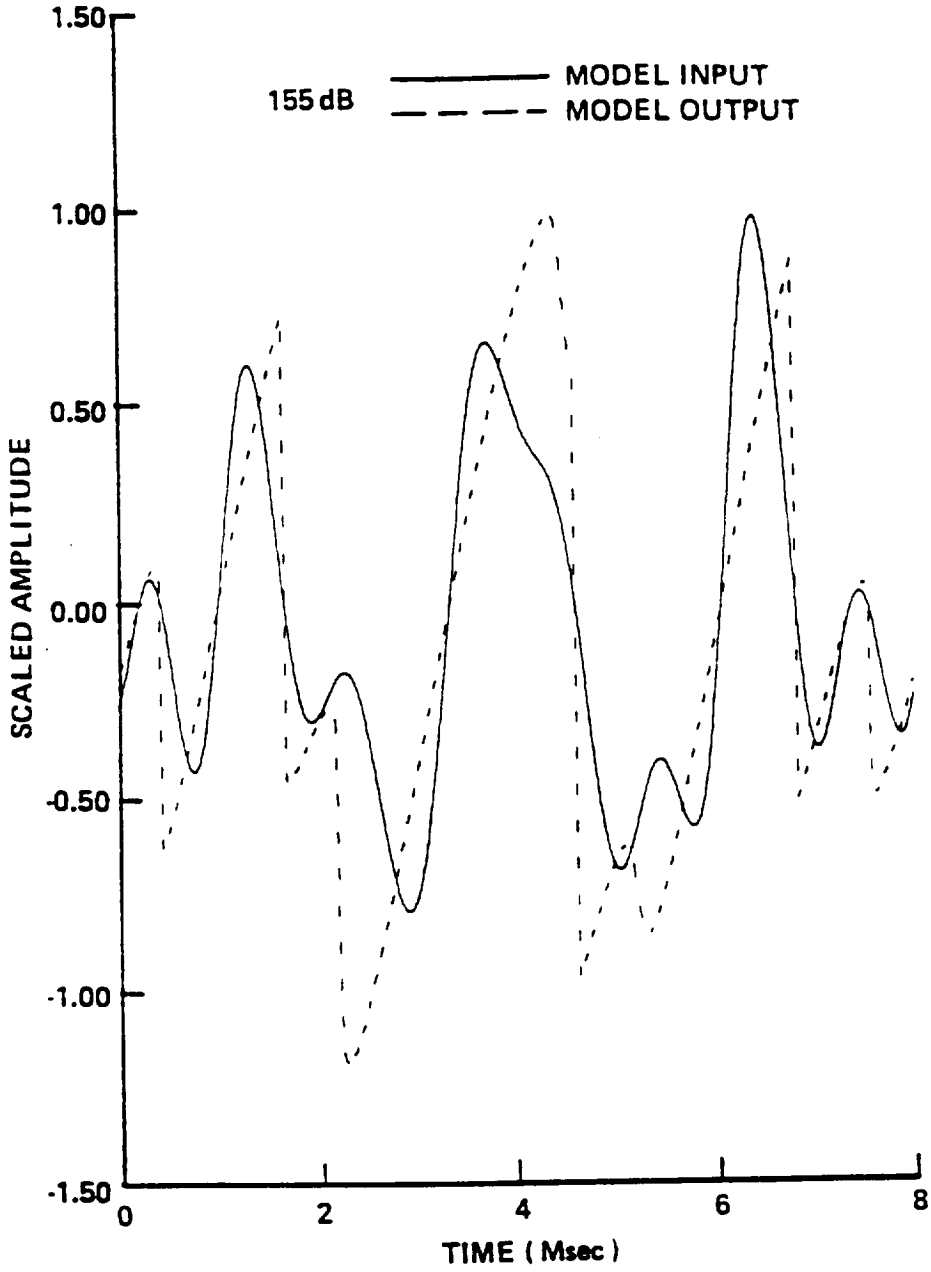

Figure 4.19 Model Output at 2.0 Meters for a 155 dB Random Noise Waveform

Discussion of Results

The results presented here show that the waveform distortion observed in the experiments are caused by acoustic phenomena. A simple model produced qualitative results that are surprisingly accurate. The model could be improved to account for the losses that are encountered in the propagation of sound in air.

Although it was not tested at very long ranges, the model could serve as a basis of a model to predict flyover noise of jets and rockets that emit high intensity noise levels. A model such as this could aid designers in determining which frequencies of the jet engines should be suppressed to meet noise regulations around airports.

CHAPTER 5

CONCLUSIONS

The purpose of this research was to observe the nonlinear distortion of spherically diverging acoustic noise, and to determine that the observed effects are indeed due to acoustic phenomena. The measurements clearly showed distortion effects in the range of 0.4 to 2.0 meters and levels in the range of 145 to 165 dB. A simple theoretical model provided evidence that the observed distortion can be predicted using acoustic principles.

The area of high intensity noise propagation is a highly complicated field. This research provides data for future researchers in the form of time history wave distortion data and spectral distortion data. It does not, and cannot, provide the answer to all of the problems of spectral distortion of high intensity jet noise.

In Chapter 2 the experimental hardware and procedures were presented. The hardware consisted of a commercially obtained acoustic high intensity source and power drive system, the input signal conditioning system, the analog signal capture system, and the digital acquisition and control system. The experimental procedures were presented in detail and included a discussion of how the FFT analyzer was utilized to capture the waveform at two points along the propagation path.

Chapter 3 presented the results of the experiment in the form of time history and spectral data. The data showed the distortion process to be dependent upon both frequency content of the noise signal and the amplitude of the signal. The data presented showed how dramatic and rapid the distortion process is at sound pressure levels above 160 dB. The spectral data showed that the distortion

process changes the slope of the noise spectrum to the shape that is observed in noise data from flyover tests of supersonic jet aircraft.

The results of modeling the distortion process were presented in Chapter 4. The theory and simplifying assumptions were presented in the beginning of the chapter. Next the model was verified by using it on pure tone data, a classical case with a known solution. The model was then exercised on three noise signals of varying intensities and the results were presented. These results are compared to measured data presented in Chapter 3 and show good agreement. It is suggested that the model can be a basis for future research and development of a noise model that could aid designers of jet engines with respect to noise control.

The measured data and predictions showed that the high frequency anomalies observed in supersonic jet and rocket noise are caused by acoustic nonlinear distortion. This research provides data which show the rate of the distortion in the near propagation path and provides a model which can deal with the early propagation. Using this data and model, future efforts may provide answers to the question of what must be quieted in jet engines to meet noise law requirements in and around airports.

REFERENCES

1. Pernet, D. F., Payne, R. C., "Non-Linear Propagation of Signals in Air," J. Sound and Vibration, 17, 1971, 383-396.

2. Crighton, D. G., Bashforth, S., "Nonlinear Propagation of Broadband Jet Noise," AIAA Aeroacoustics Conference, 1980.

3. Rudenko, S. V., Soluyan, S. T., "Theoretical Foundations of Nonlinear Acoustics," Consultants Bureau, New York.

4. Cary, B. B., "Prediction of Finite Amplitude Waveform Distortion with Dissipation and Spreading Loss," J. Acoustic. Soc. Am., 43, 1968,1364-1372.

5. Allen, C. H., "Finite Amplitude Distortion in a Spherically Diverging Sound Wave in Air," Ph. D. Thesis, Department of Physics, The Pennsylvania State College, 1950.

6. Laird, D. T., "Spherical Sound Waves of Finite Amplitude," Ph. D. Thesis, Department of Physics, The Pennsylvania State University, 1955.

7. Pernet, D. F., Payne R. C., "Propagation of Finite Amplitude Noise in Tubes," National Physical Laboratory, NPL Aero Report AC 48 , 1971.

8. Webster, D. A., Blackstock, D. T., "Collinear Interaction of Noise with a Finite Amplitude Tone," J. Acoustic. Soc. Am., 63, 1978, 687-693.

9. Webster, D. A., Blackstock, D. T., "Experimental Investigation of Outdoor Propagation of Finite-Amplitude Noise," NASA Contractor Report, 2992, 1978.

10. Webster, D. A., Blackstock, D. T., "Experimental Investigation of Outdoor Propagation of Finite-Amplitude Noise," Applied Research Laboratories, The University of Texas at Austin, ARL-TR-78-31, 1978.

11. Ling EPT-200 Owners Manual, Ling Loudspeaker Corporation, Palo Alto California, 1978

12. Seiner, J. M., "The Distribution of Jet Source Strength Intensity by Mean of a Direct Correlation Technique," Ph. D. Thesis, Department of Aerospace Engineering, The Pennsylvania State University, 1974.

13. McKendree, F. S., "A Numerical Solution of the Second-Order-Nonlinear Acoustic Wave Equation in One and Three Dimensions," Ph. D. Thesis, Department of Acoustics, The Pennsylvania State University, 1981.

14. Bellman, R., Azen, S. P., Richardson, J. M., "On New and Direct Computational Approaches to Some Mathematical Models of Turbulence,", Quart. Appl. Math, 39, 1966, 55-67.

15. Kokhlov, R. V., "The Theory of Radio Shocks in Nonlinear Transmission Lines," Radio Electronika, 6, 1961, 817-824.

16. Naugol'nykh, K., Soluyan, S. I., Khokhlov, R. V., "Spherical Waves of Finite Amplitude in a Viscous Thermally Conducting Medium," Soviet Phys.-Acoustics, 1963, 9, 42-46.